Iterative Bleaching Extends Multiplexity (IBEX) imaging facilitates simultaneous identification of all cell types in the vertebrate retina

Aanandita Kothurkar[1,§], Gregory S. Patient[1,§], Nicole C. L. Noel[1], Aleksandra M Krzywańska[1], Brittany J. Carr[2], Colin J. Chu[1,*], Ryan B. MacDonald[1,*]

§ These authors contributed equally to this work

*Co-corresponding senior authors: CJC (colin.chu@ucl.ac.uk) and RBM (ryan.macdonald@ucl.ac.uk)

[1]Institute of Ophthalmology, University College London, London EC1V 9EL, UK

[2]Department of Ophthalmology and Visual Sciences, University of Alberta, Edmonton, AB, Canada T5H 3V9

Keywords: immunohistochemistry, zebrafish, development, neurons, glia

ABSTRACT

The vertebrate retina is a complex multicellular tissue made up of distinct neuron types and glia, arranged in a stereotypic layered organisation to facilitate vision. Understanding how these cell types come together to form precise circuits during development requires the ability to simultaneously discriminate between multiple cell types and their spatial position in the same tissue. Currently, we have a limited capacity to resolve all constitutive cell types and their relationships to one another due to our limited ability to combine multiple cellular markers. To extend this capacity, we have adapted a highly multiplexed immunohistochemistry technique known as Iterative Bleaching Extends Multiplexity (IBEX) and applied it to the development of the zebrafish (*Danio rerio)* retina. IBEX allows for multiple rounds of cellular labelling to be performed, before imaging and integration of data, resulting in the ability to visualise multiple markers on the same tissue. We have optimised IBEX in zebrafish using fluorescent micro-conjugation of known antibody markers to label the complete retina with up to 11 cell-specific antibodies. We have further adapted the IBEX technique to be compatible with fluorescent transgenic reporter lines, *in situ* hybridisation chain reaction (HCR), and wholemount immunohistochemistry (WMIHC). We then took advantage of IBEX to explore the multicellular relationships in the developing retina between glial cells and neurons and photoreceptor subtypes. Finally, we tested IBEX on retinas from the emerging ageing model, the killifish (*Nothobranchius furzeri)*, and developmental model, the African clawed frog (*Xenopus laevis),* demonstrating the usefulness of the technique across multiple species. The techniques described here can be applied to any tissue in any organism where antibodies are readily available to efficiently explore cellular relationships in the context of development, ageing or disease.

INTRODUCTION

Tissues are made up of multiple cell types with regional and cell-specific molecular differences. To best understanding the relationships between these cells, and how they are altered during development, ageing and/or disease, we must have the ability to visualise the complete cellular landscape of a tissue. Our ability to do so relies on the accessibility of techniques to assay or discriminate between multiple cell types at the same timepoint using their transcriptomes, epigenomes, and/or proteomes as features to define cell states or interactions across an entire tissue (Choi *et al.*, 2023). However, techniques used to study tissue composition and cellular relationships remain in refinement and can be costly to adapt for individual tissues or species of choice. Modern techniques, such as single-cell RNA-sequencing, can identify cell-specific molecular changes in individual cells on a large scale – however, the spatial organisation of these cells is lost in processing and must be mapped back onto the tissue to maximise their value. In contrast, immunohistochemistry (IHC) techniques allow visualisation of cellular proteins expressed in specific cell types in their undisturbed locations and thus provide spatial information. The number of antibody markers and, by consequence, the amount of information that can be obtained from a single tissue sample is limited by the number of fluorophores that can be imaged at one time. This is particularly relevant where few antibodies are validated and many are raised in the same host (e.g. rabbit), and so cannot be detected at the same time. Therefore, developing techniques to map the expression of multiple cellular markers onto a tissue will enhance our ability to understand cellular state, behaviour, and function in any tissue.

The retina is the light-detecting tissue at the back of the eye, comprised of several different types of neurons and glia. Retinal structure has been well-characterised since its early description by anatomists such as Cajal, who used dye labels to identify individual cell types and their organisation based on their unique locations and morphologies (Cajal, 1893). The highly organised retina is made up of five main neuronal cell types and a principal glia cell type called

70 Müller glia (MG) (Fig. 1). Photoreceptors are the light-sensitive cells that synapse onto
71 interneurons (horizontal cells, bipolar cells, and amacrine cells) which in turn, relay and modulate
72 the signal and synapse with output neurons (retinal ganglion cells) that connect the retina to visual
73 centres in the brain via the optic nerve. These cells are organised into three discrete cell layers –
74 outer nuclear layer (ONL), inner nuclear layer (INL), and ganglion cell layer (GCL) – separated by
75 two synaptic neuropils (outer and inner plexiform layers) and form relatively simple circuits
76 (Masland, 2012). The zebrafish retina has been a useful model to study development and disease
77 as it has a conserved organisation and cellular composition with other vertebrates (Avanesov and
78 Malicki, 2010). Furthermore, it is an ideal neural tissue to image *in vivo* as the zebrafish eye is
79 transparent during embryogenesis, develops rapidly (functional by 5 days post fertilisation (dpf)
80 (Patterson *et al.*, 2013), and has a full complement of cell-specific fluorescent reporter lines to
81 visualise every cell type in the tissue (reviewed in Malicki *et al.*, 2016). Further, there are a large
82 number of antibodies with neuronal and glial specificity to discriminate different cell types and
83 visualise morphology in the vertebrate retina (such as Yazulla and Studholme, 2001). However,
84 studies of retinal development or disease remain constrained by our limited ability to combine
85 these antibodies to visualise multiple cell types and directly assay cellular relationships or states
86 in the same tissue at one time. Instead, such complex spatial information must be gathered by
87 performing IHCs with numerous combinations of the same antibody pools across many tissue
88 sections.

89 Here, we overcome these challenges by adapting and expanding the Iterative Bleaching Extends
90 Multiplexity (IBEX) technique in the vertebrate retina (Fig. 2). IBEX is a technique developed in
91 mouse and human tissues that allows simultaneous visualisation of up to 60 markers on a single
92 tissue sample (Radtke *et al.*, 2020), thereby providing large-scale, detailed multicellular spatial
93 analysis of tissue. It relies on fluorescently conjugated primary antibodies to enable use of multiple
94 antibodies raised in the same species while avoiding cross-reactivity and permits bleaching of

signal to conduct sequential rounds of immunolabelling. First, we validated “micro-conjugations” whereby a small volume of antibody is directly linked to fluorescent dyes to overcome the critical issue of multiple antibodies raised in the same species. Importantly, these fluorophores can be bleached and are compatible with multiple rounds of IHC required for the IBEX technique. Using IBEX, we then labelled every cell type in the retina with 11 specific antibody markers. We enhanced the capabilities of the IBEX technique in zebrafish by pairing with cell-specific transgenic reporter lines, wholemount IHC (WMIHC), and *in situ* hybridisation chain reaction (HCR) in zebrafish. We also use IBEX to describe the development of two key cell types in the retina: photoreceptors and MG. The techniques described here will be valuable for any tissue and are applicable to any other study where multiplexed IHC is required. Finally, to demonstrate the usefulness of IBEX across species we applied it to two additional aquatic vertebrates: the African clawed frog (*Xenopus laevis)* and the African turquoise killifish (*Nothobranchius furzeri)*. Both models are currently constrained by the lack of tools, such as few established transgenic reporter lines, making the ability to visualise multiple-cell types in the retina challenging. As such, we have adapted the IBEX technique to expand our ability to visualise multiple cell types in the same tissue sample to explore cellular relationships in the developing vertebrate retina.

RESULTS

Direct conjugation to fluorophores facilitates labelling with multiple antibodies raised in the same host on the same tissue

A major hurdle in IHC is labelling with multiple antibodies raised in the same animal (e.g. rabbit), as it would not be possible to distinguish between the antibodies using traditional secondary antibodies. To overcome this limitation, we used “micro-conjugation” reactions (see Methods) to directly link primary antibodies with distinct fluorophores, avoiding use of secondary antibodies

119 and gaining the flexibility to label each antibody with a fluorophore of choice (Fig. S1). To ensure
120 there was no cross-reactivity or quenching of signal due to competitive antibody binding, we
121 conjugated the rabbit GNAT2 antibody, which labels cone photoreceptors in the zebrafish retina,
122 with four different fluorophores. Using confocal microscopy, we observed robust signal for each
123 of the fluorophores in the photoreceptor layer with no noticeable loss of signal due to multiple
124 conjugated antibodies against the same protein (Fig. S1).

125 It is critical for the multiplexity of the IBEX technique to be able to quench the fluorescent signals
126 between rounds of IHC. We demonstrate that CoraLite fluorophores can be successfully bleached
127 using lithium borohydride ($LiBH_4$) and show a near complete loss of signal and no
128 autofluorescence in any channel post bleaching (Fig. S1). Next, to determine if we could
129 concurrently label cells with four distinct rabbit polyclonal antibodies, we micro-conjugated each
130 with different fluorophores and conducted a single round of IHC and imaging (Fig. 3). We labelled
131 cone photoreceptors with GNAT2, bipolar cell ribbon synapses with Ribeye-A, bipolar cell
132 terminals with PKC-β, and MG with RLBP1; we were able to visualise these markers concurrently
133 without any noticeable cross-reactivity. Therefore, using micro-conjugations we can reliably
134 visualise and quench the fluorophores of antibodies raised in the same species on the same
135 tissue section.

136 **Adapting IBEX to label all cell types in the zebrafish retina**

137 To label every major cell type in the retina with IHC, we designed a panel of markers against
138 proteins expressed in each cell type of the zebrafish retina composed of micro-conjugated
139 antibodies and directly conjugated antibodies. First, we optimised each antibody for use with
140 micro-conjugation by testing for bright, specific labelling in single IHC tissue staining and
141 bleaching (see Materials and Methods). In some cases, directly conjugated antibodies did not
142 show sufficient staining to be easily visualised by standard IHC or they were not successfully
143 bleached by $LiBH_4$. Fortuitously, a standard antigen retrieval step was sufficient to bleach and

144 enhance the staining for these antibodies. Using three rounds of iterative bleaching followed by
145 standard confocal imaging, we labelled each cell type in the retina using 11 markers and DAPI in
146 the same tissue section (Fig. 4, Supplementary Video 1). In each IHC round, we used DAPI to
147 label nuclei, which is used for alignment and the ultimate integration of multiple markers on the
148 same tissue as it does not bleach. This provides a consistent fiducial landmark for image
149 registration. The open source SimpleITK registration software (Radtke *et al.,* 2020) for registration
150 of confocal Z-stacks is effective at increasing the alignment of DAPI signal between the three
151 rounds (Fig. S2) and allows channels from the different rounds to be merged. As such, we
152 developed panels of combinatorial fluorescent antibody labels against each cell type in the retina,
153 imaged each panel in successive imaging rounds after quenching of fluorophores, and integrated
154 the data onto a single image file (Fig. 4A). To increase the rate at which we can acquire data from
155 multiple samples, we also optimised IBEX and the panel of markers for an epifluorescence
156 imaging system with onboard deconvolution. This allows for a large area of tissue to be imaged
157 quickly and effectively over multiple rounds to visualise 9 antibodies and a lectin stain on the same
158 tissue (Fig. S3).

159 **IBEX is compatible with cell-specific transgenic reporter lines**

160 We aimed to assess whether we could combine IBEX with existing zebrafish transgenic lines to
161 enhance our multiplex toolbox. To incorporate transgenic reporter lines into the IBEX technique,
162 it is ideal for the fluorescent protein to bleach and make the channel available for future imaging
163 rounds. We tested whether endogenous fluorescent protein signals could be quenched and then
164 re-labelled with fluorescent protein-specific antibodies by IHC. We tested several transgenic lines
165 containing cytosolic (Tg(*GFAP:GFP*),Tg(*vsx1:GFP*)^{nns5} ,Tg(*TP1:Venus-Pest*),Tg(*ptf1a:dsRed*)^{ia6}
166 ,Tg(*rho:YFP*)^{gm500}) or membrane-targeted (Tg(*tp1bglob:eGFP-CAAX*)) fluorescent proteins. We
167 found that both cytosolic and membrane-tagged GFP bleached after antigen retrieval methods
168 (Fig. S4). These transgenes could then be boosted with an anti-GFP antibody and imaged in the

169 last round of labelling. We confirmed that the transgene retained its cell specificity during this
170 process by co-labelling and observing overlapping labelling with a cell specific antibody, PKC-β
171 for Tg*(vsx1:GFP)* and GS for Tg*(tp1bglob:eGFP-CAAX) (*Fig.S4 A'',A''', B'',B'''). However, we
172 could not bleach the RFP or YFP transgenic lines with $LiBH_4$ in combination with intense light nor
173 sodium citrate antigen retrieval (Fig. S4C, D).

174 **IBEX can be combined with fluorescent *in situ* hybridisation**

175 Antibodies specific for a cell type or protein of interest can be limited in zebrafish. As an
176 alternative, *in situ* hybridisation chain reaction (HCR) is a robust method to label mRNA of interest
177 in zebrafish (Choi *et al.*, 2010, 2016, 2018). HCR has been previously combined with IHC (Howard
178 et al., 2021; Ibarra-García-Padilla et al., 2021; Ćorić et al., 2023), however, these are limited by
179 the number of channels available in a single labelling round on standard microscopes. With a
180 view to overcoming this limitation, we tested whether *in situ* hybridization chain reaction (HCR)
181 methods to label mRNA would be compatible with IBEX, such that we could conduct a multiplex
182 HCR followed by bleaching, IHC and integration of labelling techniques on the same retina. For
183 this, we performed HCR for three genes of interest: *cyp26a1*, *glula*, and *vsx1.* The expression of
184 these genes is known to be specific to different retinal cell populations: MG (*cyp26a1* and *glula*)
185 and bipolar cells (*vsx1*) (Fig. 5A-A′′′′). We then attempted to quench the signal of these
186 fluorophores using $LiBH_4$ treatment. However, we did not observe a significant reduction in signal
187 for Alexa Fluor 555 (Fig. 5B-B′′′) We were able to bleach this signal using the antigen retrieval
188 technique (Fig. 5B′′′′) before conducting a subsequent round of IHC with MG and bipolar cell
189 antibody markers (Fig. C-C′′′′). We overlayed these two rounds of imaging, one HCR and one
190 IHC, which allowed us to visualise expression of the three transcripts of interest and confirm co-
191 localisation with different retinal cell populations labelled by antibodies (Fig. 5D-D′′′′).

192 **Wholemount IBEX facilitates whole tissue labelling in zebrafish**

193 The relatively small size of the zebrafish retina and the ability to treat the fish to make them
194 optically transparent lends itself to WMIHC (Inoue and Wittbrodt, 2011; Santos, Monteiro and
195 Luzio, 2018). This technique facilitates the study of cell structure and shape in its native
196 conformation and overcomes the potential disruption of cell morphology and tissue damage
197 introduced by cryosectioning. However, the hurdle of visualizing multiple cell types in the same
198 sample remains. Therefore, we tested whether the micro-conjugated antibody staining and
199 bleaching is compatible with thicker tissues in WMIHC before carrying out the IBEX protocol. We
200 tested the protocol by immunolabelling MG and photoreceptors with two different antibodies each
201 (GS and zrf-1 for MG, and GNAT2 and blue opsin for photoreceptors), over two successive rounds
202 of imaging (Fig. 6A,A′,C,C′). Micro-conjugated antibodies penetrated the tissue and specifically
203 labelled photoreceptors and MG. Treatment with $LiBH_4$ successfully bleached the signal of each
204 of the fluorophores between rounds (Fig. 6B). The SimpleTK registration software allowed us to
205 combine the images and observe the co-localisation of antibodies labelling Müller glia and
206 photoreceptors, respectively, across different rounds of immunofluorescence (Fig. 6E,E′,F,
207 Supplementary video 2). Therefore, WMIHC when combined with IBEX allows 3D labelling of
208 multiple cell types and alignment of their spatial relationships to one another between rounds.

209 **IBEX facilitates the characterisation of retinal histogenesis and patterning**

210 The retina has a stereotyped histogenesis whereby retinal neurons and glia are born and specified
211 in distinct temporal sequence during retinogenesis (Agathocleous and Harris, 2009). Specification
212 of the zebrafish retina begins at 24 hours post fertilisation (hpf) as a retinal primordium, completing
213 histogenesis by 73 hpf (Easter and Nicola, 1996) with robust vision beginning at 5 dpf. We used
214 this well-characterised developmental pattern to determine the utility of IBEX to describe cellular
215 morphologies in the highly dynamic developing retina. We focussed on two main cell types:
216 photoreceptors, which have five distinct subtypes that are challenging to visualise simultaneously
217 by traditional methods, and MG, due to their highly dynamic morphological changes across retinal

development. We used cryosections at different key timepoints of retinal development to accomplish this.

Zebrafish photoreceptors undergo rapid development, with light-sensitive opsin mRNA expression detectable by 60 hpf (Robinson, Schmitt and Dowling, 1995). Zebrafish are tetrachromats: they have rods and four cone photoreceptor subtypes, maximally sensitive to ultraviolet (UV), blue, green, and red light. Different photoreceptor types are identifiable by specific markers; however, traditional methods make it challenging to label all photoreceptor subtypes such that they are distinguishable from one another. We combined antibody labelling with a transgenic line with fluorescently labelled rods (Tg(*rho:YFP*) line) to label all photoreceptors with subtype resolution in the developing zebrafish retina at three stages (3, 4, and 5 dpf) (Fig. 7). Of note, YFP did not bleach with LiBH4 nor antigen retrieval, and therefore antibody labelling rounds were adjusted to avoid use of 488 fluorophores. We distinguished between the cone subtypes by utilising antibodies against UV, blue, and red opsin (via 1D4), as well as arrestin 3a (with zpr-1). Zpr-1 labels both red and green cones; green cones can therefore be identified as cells that are arrestin 3a-positive but do not stain for red opsin (Fig. S6). At 3 dpf, developing cone photoreceptors stain with GNAT2 and zpr-1 (Fig. S5A″), and have small outer segments labelled with antibodies for PRPH2, UV opsin, blue opsin, and red opsin (Fig. S5A‴, A⁗). Most of the cones with discernible outer segments were observed in the central retina. Few newly developed YFP-positive rods can also be observed in the retinal periphery. By 4 dpf, cones appear more morphologically mature with lengthened outer segments (Fig. S5B-B⁗). As mentioned, zebrafish cones are functional by 5 dpf and the animals begin to perform complex visually mediated behaviours, such as prey capture (Patterson *et al.*, 2013). Corresponding with this, 5 dpf zebrafish cones have visually longer outer segments compared to 4 dpf with a tapered morphology (Fig. S5C-C⁗). Furthermore, there appear to be phagosomes in the RPE staining for zpr-1, GNAT2, UV opsin, and PRPH2, suggesting that there is outer segment disc shedding at this stage.

243 During development, nascent MG cells begin as simple unbranched radial cells at 2.5 dpf, before
244 morphologically elaborating to a mature, highly branched structure by 5 dpf (Williams *et al.*, 2010;
245 MacDonald *et al.*, 2015; Wang *et al.*, 2017). MG are among the last retinal cell types to mature,
246 integrating into neuronal circuits when neurons are undergoing robust synaptogenesis (Cepko *et*
247 *al.*, 1996). To determine MG specification relative to development of other retinal neurons and
248 inner plexiform layer (IPL) formation, we used markers for MG: Zrf-1 (recognising Gfap),
249 glutamine synthetase (GS), and the Tg(*Tp1:EGFP-CAAX*) transgenic reporter line, which labels
250 retinal progenitors and MG (MacDonald *et al.*, 2015; Kugler *et al.*, 2023). We labelled amacrine
251 cells and retinal ganglion cells with HuC/D, horizontal cells with CA-1, bipolar cells with PKC-β,
252 and synapse formation with Ribeye-A. We observed retinal progenitors at 2 dpf (Fig. 7A-A‴)
253 labelled by the GFP transgene, corresponding to retinal ganglion cell (RGC) specification below
254 the IPL, before MG genesis and onset of MG cell body basal migration at 2.5 dpf. MG are labelled
255 by the transgene and zrf1 at 2.5 dpf, but GS labelling is not yet apparent (Fig. 7B-B‴). At this
256 point, the nascent IPL is present, as evidenced by the separation of the HuC/D signal and
257 presence of ribbon synapses (Ribeye-A) (Fig. 7B′,B‴). From this timepoint, horizontal cells are
258 visible, marked by carbonic anhydrase (CA) below the outer plexiform layer (Fig. 7B′,C′,D′). At 3
259 dpf, IPL expansion and bipolar cell terminal stratification is seen (Ribeye-A and PKC-β), along
260 with the beginning of organisation of the IPL into clear sub-laminae (Fig. 7C′-C‴). Additionally,
261 MG cell bodies have migrated to their final positions (Fig. 7C″) and are marked by GS labelling.
262 By 5 dpf, the ribbons are organised into discrete layers in the IPL, with a visible separation
263 between the ON and OFF layers and MG have elaborated processes into this layer to provide
264 homeostatic support functions (Fig. 7D-D‴). As such, we used IBEX to describe retinal
265 histogenesis, neuron migration and patterning relative to glial specification and morphogenesis
266 across retinal development in the zebrafish. In conclusion, we were able to employ the IBEX
267 technique and specifically designed antibody panels to describe multiple cell types at key stages

268 of retinal development to explore their cellular relationships, which would not be possible with
269 traditional methods.

270 **IBEX on frog and killifish retina tissues**

271 To verify the versatility of the IBEX technique across various animal models, we conducted IBEX
272 on retinas of *Xenopus laevis* tadpoles and adult African turquoise killifish. We performed IBEX on
273 tadpole retinas to label different retinal cell types using HuC/D, PAX6, GS, GαO, cone opsin (CO),
274 and zpr-3 antibodies (Fig. 8A, Supplementary Video 3). HuC/D labelled cells within the INL, GCL,
275 as well as photoreceptor inner segments. PAX6 labelled cells within the GCL – either displaced
276 amacrine cells or RGCs – while GS labelled Müller glia. GαO labelled bipolar cell bodies and
277 densely labelled processes within the IPL. L/M cone outer segments were labelled with both CO
278 and zpr-3. The CO antibody was raised against red opsin (lws), while zpr-3 is an anti-rhodopsin
279 antibody which labels the green cone opsin (rhodopsin 2). IBEX was further conducted on the
280 retinas of 8-week-old adult male African turquoise killifish (Fig. 8B, Supplementary video 4). As
281 expected, calretinin immunoreactivity was observed in retinal ganglion cells and horizontal cells.
282 HuC/D and PAX6 labelled amacrine and retinal ganglion cells and partial overlap of two markers
283 was observed. Zpr-1 labelled entire double cone cells, whereas PRPH2 expression was seen in
284 photoreceptor outer segments. Both GS and Zrf-1 (recognizing Gfap) labelled MG cells. PCNA
285 serves as an endogenous histologic marker for the G1/S phases of the cell cycle, therefore PCNA
286 expression serves as a marker of cell proliferation. In killifish retina, PCNA was densely expressed
287 in the ciliary marginal zone (CMZ) and signal was also observed in the ONL. The pan-leukocyte
288 marker Lcp-1 was observed in the INL, close to the CMZ, and within the ONL. As such, we have
289 demonstrated that the IBEX techniques will translate to any other tissue where multiple antibodies
290 are available.
291

292 **DISCUSSION**

293 There is a lack of tools available to discriminate between more than three to four cell types in a
294 tissue simultaneously. Here, we adapted the IBEX technique to vertebrate tissues and optimised
295 the methodology to be compatible with zebrafish cell-specific fluorescent reporter lines,
296 wholemount IHC, and *in situ* HCR. Further, we employed IBEX to describe the relationships
297 between glial cells and neurons and explore the entire complement of photoreceptor subtypes in
298 the developing zebrafish retina. Additionally, we utilised IBEX to characterise the retina in killifish
299 and *Xenopus laevis.* Therefore, IBEX is a robust method to multiplex markers and characterise
300 cellular and molecular processes in the vertebrate model organisms.

301 **IBEX complements the existing zebrafish toolkit**

302 We show that it is possible to combine IBEX with available transgenic lines with fluorescent protein
303 expression. Zebrafish have a wealth of cell-specific transgenic reporter lines that drive transgene
304 expression in each population of retinal cell. These have been valuable tools to characterise the
305 development and degeneration of retinal cell types in many studies (Fadool, 2003; Bernardos and
306 Raymond, 2006; Zolessi *et al.*, 2006; Kimura, Satou and Higashijima, 2008; Vitorino *et al.*, 2009;
307 Almeida *et al.*, 2014). We found that different fluorescent proteins have different bleaching
308 success, with GFP bleaching reliably and RFP and YFP not bleaching. BFP or CFP were not
309 assessed. Thus, it is possible to pair IBEX with transgenic lines, although this should be tested
310 on a case-by-case basis to determine whether endogenous fluorescent proteins can be bleached,
311 and subsequent labelling rounds adjusted accordingly. Antibodies specific for a cell type or protein
312 of interest can be limited in non-mammalian species, and this is especially true for poorly studied
313 or newly discovered genes. Further, studies may be interested in assessing spatial localisation of
314 noncoding RNAs within tissues. As an alternative to antibody labelling, *in situ* hybridisation chain
315 reaction (HCR) is a robust method to label mRNA of interest (Choi *et al.*, 2010, 2016, 2018). We
316 novelly combined *in situ* HCR with IBEX to spatially localise transcript expression for three genes
317 with cellular markers across two cell types (three antibody labels). This can be applied to other

318 systems to determine with high resolution which cell populations are expressing transcript for a
319 gene of interest. Hence, combining *in situ* HCR with IBEX is a powerful technique to identify
320 expression patterns of genes of interest by localizing gene expression to different immunolabelled
321 cell types. WMIHC is an effective technique to study the expression pattern of proteins while
322 preserving the 3D structure of the tissue. IBEX allows us to conduct multiple rounds of WMIHC
323 on the same tissue. This greatly increases the amount of information we can obtain from a single
324 tissue, is a useful extension of WMIHC to simultaneously visualise multiple proteins in their native
325 location in tissues and explore the spatial relationships between different cell types in whole intact
326 tissues.

327 **Antibody panel design and considerations**

328 To maximise the potential of IBEX, we developed panels to label as many cell types as possible
329 in each round of IBEX. Careful planning is required to design panels of markers
330 (antibodies/lectins) to be used based on previous individual reactions and bleaching tests. The
331 brightest and least efficiently bleached markers, for instance lectins or transgenes, were used in
332 later or, ideally, last round to minimise the potential for significant leftover signal. Similarly, the
333 weakest markers were used in early panels to increase the likelihood of strong signal detection.
334 It is important to note that certain fluorophores are more amenable to bleaching than others, and
335 later rounds are more susceptible to autofluorescence, particularly in the 555 channel (as in Fig.
336 4 and supplemental Fig. 5), where some residual inner retinal staining is observed while labelling
337 with GNAT-2. We ensured that the fluorophores which have been validated to bleach in the
338 original protocol (Radtke et al., 2020) were used and any new fluorophores, such as the CoraLite®
339 Plus, were tested for bleaching prior to use in IBEX (Fig. 3F). It is possible to use secondary
340 antibodies in IBEX, and this may be required for antibodies that fail to efficiently label via micro-
341 conjugation. However, these secondaries must be incorporated into the first round of the IBEX if
342 recognising a species from which multiple antibodies within the designed panel are raised, as

343 subsequent rounds using antibodies raised in that same species will lead to cross-reactivity; in
344 the case that there is a single antibody from a specific species within the panel, the antibody can
345 be incorporated into any round using secondary antibodies. For most fluorophores, incubation
346 with $LiBH_4$ before washing was sufficient for bleaching the fluorophore. However, in some cases
347 it required an antigen retrieval step (i.e. heating in sodium citrate) which efficiently quenches
348 fluorophores. Importantly, after the antigen retrieval and IBEX procedure on zebrafish retinal
349 tissue, the nuclei appeared qualitatively similar across three rounds of IHC and imaging (Fig. S2)
350 and were easily aligned using the SimpleITK registration software.

351 **Potential of IBEX and multiplexing in other species**

352 IBEX can also be applied to any species where multiple cell-specific antibodies, fluorescent
353 reporter transgenes, and/or fluorescent *in situ* hybridisation techniques are available. However,
354 these techniques and antibody panels will need to be validated on a case-by-case basis. These
355 methodologies, some developed here, will be especially valuable where multiple different markers
356 are required to confirm the identity of a cell, such as immunological studies. We also demonstrate
357 the benefits of IBEX to characterise multiple cell types in unconventional model organisms, such
358 as the killifish and *Xenopus laevis,* in which there are few transgenic reporter lines. IBEX allows
359 us to maximise the information that can be obtained from a single piece of tissue, a huge benefit
360 for study of rare species or tissue that is difficult to access. Furthermore, it can be used to
361 potentially identify subpopulations that would not be possible with conventional IHC in such
362 organisms. Labelling multiple markers on the same tissue will also have important implications
363 for animal ethics and 3Rs (Replacement, Reduction, and Refinement) initiatives as the number
364 of animals required for statistically significant phenotypic data is greatly reduced. Performing
365 multiple rounds of IHC on the same tissue produces rich datasets where the interactions between
366 multiple cell types can be explored. As such, multiplexing techniques are not only powerful for

367 exploring cellular relationships but also critical for efforts to reduce animal numbers in scientific
368 research.

369 **Limitations and future work**

370 There were some limitations to the IBEX approach. Micro-conjugations can be unreliable on
371 occasion (i.e. not all antibodies successfully conjugate), there is a need for a relatively large
372 volume of validated primary antibody (although much less than when performing a primary
373 conjugation), and the technique works most effectively when the protein in question is highly
374 abundant. Hence, when used for proteins that have low expression or low affinity for antibodies,
375 the concentrations may have to be increased over traditional methods. Many antibodies do not
376 have their exact antigen identified or validated in non-mammalian systems, such as zebrafish.
377 However, as we were only looking at broad cell type distributions, rather than targeted molecular
378 events, validation of each antigen was not necessary for this study. When possible, we did utilise
379 antibodies with known/validated antigens. When using unvalidated antibodies, we selected those
380 that had conserved labelling patterns and included other methods – such as transgenic lines and
381 *in situ* hybridisation – to complement the labelling and provide information about specificity.
382 Transgenic lines with RFP/YFP that do not bleach (such as the Tg(*rho:YFP*) line used for the
383 developmental series in Fig. 7) can still be used if required but would reduce the number of
384 channels available for successive imaging rounds. Finally, there are likely limitations on the
385 number of immunolabelling rounds that can be performed without tissue damage or visible
386 residual signal from previous rounds. However, we have conducted four rounds of IBEX on retinal
387 cryosections and there has been no noticeable degradation of tissue integrity or signal loss. As
388 such, it may be possible to >20 markers on a single zebrafish cryosectioned tissue, as there have
389 been 20 rounds and 66 antibodies reported in human lymph nodes (Radtke *et al.*, 2020).

390 The IBEX technique is compatible with standard confocal as well as epifluorescence microscopy.
391 Here, we principally used a standard confocal microscope with four excitation laser wavelengths

392 (405, 488, 555, and 647) that allowed a maximum of three antibodies plus DAPI in each panel.
393 However, this can be expanded upon if your microscope has additional spectral capabilities (e.g.
394 tuneable or white light laser) and antibodies are visualised with additional fluorophores via
395 conjugation or secondary antibodies. To this end, we also conducted IBEX using an
396 epifluorescence microscope with Z-stack capabilities and expanded spectral excitation properties
397 to visualise 10 markers on the same tissue (Fig. S3). As such, this technique will be applicable to
398 any fluorescence microscopes available where multiple channels can be acquired on the same
399 tissue.

400 In conclusion, this technique can be a powerful method to explore cellular relationships and
401 biological processes in complex multicellular tissues in the context of development, ageing or
402 disease.

403

404 **MATERIALS AND METHODS**

405 **Table 1.** Antibodies used for immunohistochemistry and IBEX.

Primary antibodies					
REAGENT OR RESOURCE	**CELLULAR TARGET IN ZEBRAFISH**	**HOST**	**SOURCE**	**IDENTIFIER**	**DILUTION**
α-1D4	Red cone Photoreceptors	Mouse monoclonal	Santa Cruz Biotechnology	Cat. No. sc-57432	1:50

α-ARR3	Cone photoreceptors	Rabbit polyclonal	Merck	Cat. No. AB15282	1:50
α-Blue opsin	Blue cones	Rabbit polyclonal	Kerafast	Cat. No. EJH012	1:50
α-Calbindin	Amacrine cell subpopulation, Retinal ganglion cells	Rabbit	Swant	Cat. No. CB38a	1:50
α-Calretinin	Amacrine cells subpopulation, Retinal Ganglion cells	Rabbit polyclonal	Swant	Cat. No. 7697	1:150
α-Carbonic anhydrase	Horizontal cells and Müller glia subpopulation	Rabbit polyclonal	ABCAM	Cat. No. ab108367	1:50
α-cone opsin (lws, *Xenopus*)	N/A	Rabbit	N/A	N/A	1:200
α-GαO	N/A	Mouse	EMD Millipore	MAD3073	1:200
α-GFAP	Müller glia	Mouse	Biolegend	Cat. No. 837508	1:50
α-GFP	GFP	Rabbit polyclonal	Invitrogen	Cat: A11122	1:500
α-GNAT2	Cone photoreceptors	Rabbit polyclonal	MBL	Cat. No. PM075	1:75

α-GS	Müller glia	Mouse	Proteintech	Cat. No. CL488-66323	1:50
α-HuC/D	Amacrine cells and Retinal Ganglion cells	Mouse	Invitrogen	Cat. No. A21271	1:100
α-LCP1	Macrophages	Rabbit polyclonal	Proteintech	Cat. No. 13025-1-AP	1:50
α-LCP1	Macrophages	Rabbit polyclonal	GeneTex	Cat. No. GTX124420	1:50
α-M/L opsin	Cone photoreceptors	Rabbit	Millipore Merck	Cat. No. AB5405	1:50
α-PAX6	Amacrine cells	Rabbit polyclonal	Proteintech	Cat. No.	1:50
α-PCNA	Proliferating cells	Rabbit polyclonal	Proteintech	Cat. No. 24036-1-AP	1:50
α-PCNA	Proliferating cells	Mouse monoclonal	Santa Cruz Biotechnology	Cat. No. SC-56	1:50
α-PKC-β	Rod bipolar cells and their terminals	Rabbit Polyclonal	Proteintech	Cat. No. 12919-1-AP	1:50
α-PRPH2	Photoreceptors	Rabbit polyclonal	Proteintech	Cat. No. 18109-1-AP	1:200

α-Ribeye-A	Bipolar cell ribbon synapses	Rabbit polyclonal	Gift from Teresa Nicholson	NA	1:500
α-RLBP1	Müller glia	Rabbit polyclonal	Proteintech	Cat. No. 15356-1-AP	1:50
α-RPE65	Retinal pigment epithelium	Rabbit polyclonal	Proteintech	Cat. No. 17939-1-AP	1:25
α-UV opsin	UV cone photoreceptors	Rabbit polyclonal	Kerafast	Cat. No. EJH013	1:50
α-Zo1	Tight junctions	Mouse Monoclonal	Life technologies	Cat. No. 339100	1:150
α-Zpr1	Double cone photoreceptors	Mouse	ZIRC	ZDB-ATB-081002-43	1:200
Zpr-3	Green cone photoreceptors, rod photoreceptors	Mouse	ZIRC		
α-Zrf-1	Müller glia basal end	Mouse Monoclonal	ZIRC	Cat. No. ZDB-ATB-081002-46	1:25
Secondary antibodies					
α-Rabbit Alexa Fluor™ 647		Goat	Invitrogen	Cat. No. A-21244	1:1000

α-Rabbit Alexa Fluor™ 546		Goat	Invitrogen	Cat. No. A-11035	1:1000
α-Mouse Alexa Fluor™ 546		Goat	Invitrogen	Cat. No. A-11030	1:1000
α-Mouse Alexa Fluor™ 647		Goat	Invitrogen	Cat. No. A-21235	1:1000
α-Chicken Alexa Fluor™ 488		Goat	Invitrogen	Cat. No. A-11039	1:1000
Other markers					
Lectin PNA			Invitrogen	Cat. No. L21409	
DAPI			Invitrogen	Cat. No. D1306	1:1000
Conjugation kits					
FlexAble CoraLite® 488 Antibody Labeling Kit for Rabbit IgG			Proteintech	Cat. No. KFA001	
FlexAble CoraLite® Plus 550 Antibody Labeling Kit for Rabbit IgG			Proteintech	Cat. No. KFA002	

FlexAble CoraLite® Plus 647 Antibody Labeling Kit for Rabbit IgG			Proteintech	Cat. No. KFA003	
FlexAble CoraLite® Plus 750 Antibody Labeling Kit for Rabbit IgG			Proteintech	Cat. No. KFA004	
FlexAble CoraLite® Plus 550 Antibody Labeling Kit for Mouse IgG1			Proteintech	Cat. No. KFA022	
FlexAble CoraLite® Plus 647 Antibody Labeling Kit for Mouse IgG1			Proteintech	Cat. No. KFA023	
ReadiLink™ Rapid iFluor® 594 Antibody Labeling Kit			AAT	Cat. No. 1230-AAT	

407 **Animals**

408 Adult fish were housed in the animal facility at the University College London on a 14:10 hour
409 light/dark cycle at 28°C, following previously established husbandry protocols (Westerfield, 1993).
410 Experimental procedures were conducted in accordance with the UK Home Office Animals
411 (Scientific Procedures) Act 1986 (zebrafish project license PPL: PP2133797, held by R.B.M, and
412 killifish PPL: PP7179495 held by Dr Elspeth Payne). Zebrafish embryos were obtained by light-
413 induced spawning, collected in E3 buffer (5 mM NaCl, 0.17 mM KCl, 0.33 mM CaCl2, 0.33 mM
414 MgSO4) with/without methylene blue, and maintained in an incubator at 28.5°C till use.

415 *Xenopus laevis* (African clawed frog) use was approved by the University of Alberta Animal Use
416 and Care Committee (AUP00004203) and carried out in accordance with the Canadian Council
417 on Animal Care. Frogs were housed at 18°C under a 12-hour cyclic light schedule (7:00-19:00;
418 900-1200 lux).

419 **Animal strains**

420 Wildtype zebrafish embryos (ABTL/Tübingen) were used for the adaptation of the IBEX technique
421 on section IHC, WMIHC and combined HCR/IHC. Tg(*GFAP:GFP*) (Bernardos and
422 Raymond,2006), Tg(*vsx1:GFP*)^{nns5} (Kimura, Satou and Higashijima, 2008), Tg(*TP1:Venus-Pest*)
423 (Ninov, Borius and Stainier, 2012), Tg(*tp1bglob:eGFP-CAAX*) (Kugler *et al.*, 2023) and
424 Tg(*ptf1a:dsRed*)^{ia6} (Jusuf *et al.*, 2012) were used to optimise the protocol for IBEX using
425 transgenics. Tg(*rho:YFP*)^{gm500} (White *et al.*, 2017), Tg(*tp1bglob:eGFP-CAAX*) embryos were used
426 at different timepoints to study development of neurons and glia. Wild type killifish adults (GRZ)
427 and wild type *Xenopus laevis* were used for adaptation of IBEX on retinal sections.

428 **Preparation of retinal sections**

429 Animals at the desired stages were overdosed with 0.4% Tricaine and fixed in 4%
430 paraformaldehyde overnight at 4°C. Tissues were washed 3 times for 5 min in PBS and then

431 immersed in either 20% (frogs) or 30% (fishes) sucrose in PBS and allowed to sink overnight.
432 Samples were embedded in OCT (Sigma Aldrich, Cat. No. SHH0024) and frozen at -80°C. Frog
433 eyes were obtained by B.J.C. Froglets aged 145 days post-fertilization were euthanised by
434 overdose with tricaine (0.5% until unresponsive to toe pinch), decapitation, and then pithing.
435 Whole eyes were fixed in 4% PFA + 3% sucrose overnight, cryoprotected in 20% sucrose
436 overnight with gentle shaking, and then shipped to UCL in 20% sucrose for further processing.
437 SuperFrost™ Plus Adhesion Microscope Slides (Epredia, Cat. No. J1800AMNZ) were coated
438 evenly with 5μL chrome alum gelatin (Newcomer Supply, Part# 1033C) and dried in an incubator
439 at 60°C for one hour, to minimise loss of tissue over multiple rounds of immunolabelling. Retinal
440 sections of embedded tissues were sectioned onto these slides at a thickness of 12-14 μm using
441 a cryostat (Leica CM1950) and left at room temperature (RT) to dry overnight. Slides were then
442 stored at -80°C.

443 **Antibody micro-conjugation**

444 Each antibody (Table 1) was tested with the FlexAble micro-conjugation kits at the recommended
445 concentration (0.5 μg) per slide. However, this did not label cells efficiently in retinal sections.
446 Doubling the concentration of primary antibody was found to stain tissue more effectively. 1 μg of
447 each primary antibody was combined with 2 μL of FlexAble linker protein for the desired
448 fluorophore, and the volume was made up to 16 μL with the provided buffer, following kit
449 recommendations. This solution was incubated for 5 minutes in the dark at RT, and then 4 μL of
450 quencher was added and left to incubate in the dark at RT for a further five minutes, according to
451 the manufacturer's protocol. The entire reaction volume for each antibody was used for
452 subsequent steps.

453 **IBEX technique**

454 This method is an adapted version of the original IBEX protocol (Radtke *et al.*, 2020) and an
455 overview is given in Fig. 2. The sections were rehydrated in PBS for 5 minutes at RT. Antigen
456 retrieval was then performed by heating the slides for 20 minutes in 10 mM sodium citrate (pH 6).
457 This step quenched the signal in most of the zebrafish GFP transgenic lines tested, but the GFP
458 can be boosted in later rounds of immunolabelling using a primary antibody against GFP. The
459 sections were blocked for 1 hour in block solution (10% goat serum, 1% BSA, 0.8% Triton X, 0.1%
460 Tween, made up with PBS) at RT. Primary antibodies were conjugated to fluorophores as
461 described above. The slides were incubated with of the first round of antibodies, diluted
462 appropriately in block solution, at 4°C overnight. Following three 20-minute washes with PBS,
463 secondary antibodies were added, if needed. Slides were then incubated at RT for two hours or
464 overnight in 4°C and washed after with PBS three times for 10 minutes. Slides were mounted in
465 Fluoromount G mounting media (Cat. No. 00-4958-02, Invitrogen) and imaged on a Leica
466 THUNDER imager, Leica SP8 confocal microscope, or Zeiss LSM 900 inverted confocal using 4-
467 5 channels: 405, 488, 550, 647 and 750 nm.

468 After image acquisition, slides were placed in a 50 mL falcon tube filled with PBS and left until the
469 coverslip fell off, and then washed three times to remove the mounting media. Fluorophores were
470 quenched by incubating slides in 150 µL of lithium borohydride ($LiBH_4$, 16949-15-8, STREM)
471 solution (1-2 mg/mL) under direct white light (minimum of 300 lux). The slide was then washed
472 three times for 10 minutes in PBS before the next round of antibodies was added and steps were
473 repeated as above.

474 **IBEX for combined *in situ* HCR/IHC on sections**

475 HCR probes for *cyp26a1* and *vsx1* were kindly gifted by Takeshi Yoshimatsu, while the probe set
476 for *glula* was designed using a custom script (Trivedi and Powell, unpublished) and ordered from
477 Life Technologies, ThermoFisher. HCR amplifiers (Alexa Fluor 488, Alexa Fluor 546, and Alexa

478 Fluor 647), and buffers (hybridisation, wash, and amplification) were purchased from Molecular
479 Instruments (https://www.molecularinstruments.com/). A published *in situ* HCR protocol (Choi *et*
480 *al.*, 2018) was adapted for retinal zebrafish sections. Slides were rehydrated in PBS for 5 minutes
481 and then treated with 250 µL proteinase K (20µg/mL) for 10 minutes at RT. They were washed
482 twice with PBS + 0.1% Tween (PBST) and post-fixed with 250 µL of 4% paraformaldehyde for 20
483 minutes at RT. Slides were washed 3 times for 5 minutes with PBST and incubated in 150 µL of
484 probe hybridisation buffer at 37°C for 30 minutes. Sections were then incubated overnight at 37°C
485 in probe solution (4 µL of each probe set, made up to 150 µL in probe hybridisation buffer). Excess
486 probes were removed by washing slides 4 times for 15 minutes in probe wash buffer at 37°C, and
487 then 2 times for 5 minutes with 5X SSCT buffer at RT. Slides were pre-amplified in 150 µL of
488 amplification buffer for 30 minutes at RT. 4 µL each of hairpin 1 and hairpin 2 amplifier were snap
489 cooled by heating to 95°C for 90 seconds and cooling to RT. These were then added to the slides
490 in 150 µL of amplification buffer and incubated overnight at RT in the dark. Slides were washed 4
491 times for 5 minutes in 5X SSCT buffer and mounted in Fluoromount G media. Sections were
492 imaged on the Zeiss LSM 900 with a 40x immersion oil objective (Na 1.1) using 4 channels: 405,
493 488, 546, and 647 nm. After image acquisition, slides were heated to 60°C in sodium citrate (pH
494 6) for 20 minutes to quench fluorophores. IHC was then repeated on sections as described above.

495 **IBEX for WMIHC**

496 Wildtype zebrafish embryos were treated with 0.0045% phenylthiourea from 6 hpf to prevent
497 pigment formation and at 5 dpf, were overdosed with 0.4% Tricaine and fixed in 4%
498 paraformaldehyde overnight at 4°C. They were washed in PBST and heated in 10mM sodium
499 citrate (pH 6) at 70°C for 15 minutes. Samples were washed twice for 10 minutes in PBST, twice
500 for 5 minutes in distilled water and incubated with ice cold acetone for 20 minutes at -20°C. This
501 was followed by three 5 min washes in PBS and incubation in blocking solution (10% goat serum,
502 0.8% Triton X-100, 1% BSA in PBST) for 2 hrs at RT. Micro-conjugation of the antibodies was

503 carried out as described above, doubling the volume of antibody used for sections. Embryos were
504 incubated in antibody solution with DAPI, diluted with blocking solution, at RT overnight with
505 gentle agitation at room temperature. After three 1-hour washes in PBS + 1% Tween, embryos
506 were mounted in molten 1% low melting point agarose in PBS, in a glass bottomed dish. Once
507 hardened, they were covered with 1X PBS and imaged on the Zeiss LSM 900 with a 40x
508 immersion oil objective (Na 1.1) using 4 channels: 405, 488, 546, and 647 nm. Embryos were
509 then extracted from the agarose and bleached with $LiBH_4$ solution mentioned above in individual
510 tubes for 2 hours at room temperature. The antibody incubation process was repeated, keeping
511 embryos separate in order to overlay correct images during registration. They were then imaged
512 as mentioned above, keeping imaging parameters like stack size and step size consistent
513 between rounds.

514 **Optimization of quenching of fluorophores**

515 Fluorophores react differently to bleaching with $LiBH_4$, and therefore, we used several different
516 methods to bleach signal between rounds of labelling. CoraLite micro-conjugated antibodies
517 bleached after 30 minutes of $LiBH_4$ treatment under bright light. The same antibodies required 2
518 hours of incubation in $LiBH_4$ solution to observe reduction in signal in WM IHC. In cases where
519 Alexa Fluor 555 secondary antibody was used, 30 minutes of heating at 60°C in sodium citrate
520 solution (pH 6) was needed to quench the fluorescence. For transgenic lines, antigen retrieval by
521 boiling slides in sodium citrate solution (pH 6) for 20 minutes quenched the fluorescent protein,
522 but when boosted with the anti-GFP primary and Alexa Fluor secondary antibodies, the signal
523 was not reduced even after antigen retrieval. Hence, fluorophores must be individually tested to
524 assess suitability for use with IBEX, and ones that do not show reduction in signal used in the last
525 round of immunolabelling.

526 **Image processing and alignment**

527 Imaging parameters such as stack size, number of steps, step size, scan speed, and resolution
528 were kept consistent across all rounds of imaging. Once all rounds were completed, Imaris
529 (Oxford Instruments) was used to process the images. Brightness, contrast, and colours were
530 adjusted and filters, such as Gaussian, were applied where appropriate. Once all images were
531 processed, the SITK-IBEX registration code (Radtke *et al.*, 2020) was used to register them, using
532 DAPI as the alignment channel. Maximum projection images were obtain using the snapshot
533 feature while in 3D viewer or by using the orthogonal slicer tool.

534

535 **ACKNOWLEDGEMENTS**

536 We would like to thank Dr. Mariya Moosajee for the kind gift of *Tg(rho:YFP)*^{gm500} embryos, and
537 Dr. Chintan Trivedi for allowing use of his custom HCR probe design script. We also thank Dr.
538 Elspeth Payne for providing access to killifish tissue and UCL BRU staff for care and maintenance
539 of animals used in this study. This study was supported by BrightFocus Macular Degeneration
540 Postdoctoral Fellowships to N.C.L.N. (M2022002F) and B.J.C. (M2021001F), University of
541 Alberta startup funds to B.J.C, a Wellcome Trust Clinical Research Career Development
542 Fellowship (224586/Z/21/Z) and Moorfields Eye Charity equipment grant to C.J.C and a BBSRC
543 David Phillips Fellowship (BB/S010386/1) and a Moorfields Eye Charity PhD Studentship
544 (GR001503) to R.B.M.

545

546 **REFERENCES**

547 Agathocleous, M. and Harris, W.A. (2009) 'From Progenitors to Differentiated Cells in the
548 Vertebrate Retina', *Annual Review of Cell and Developmental Biology*, 25(1), pp. 45–69. Available
549 at: https://doi.org/10.1146/annurev.cellbio.042308.113259.

Almeida, A.D. *et al.* (2014) ‘Spectrum of Fates: a new approach to the study of the developing zebrafish retina’, *Development*, 141(14), pp. 2912–2912. Available at: https://doi.org/10.1242/dev.114108.

Avanesov, A. and Malicki, J. (2010) ‘Analysis of the Retina in the Zebrafish Model’, *Methods in cell biology*, 100, pp. 153–204. Available at: https://doi.org/10.1016/B978-0-12-384892-5.00006-2.

Bernardos, R.L. and Raymond, P.A. (2006) ‘GFAP transgenic zebrafish’, *Gene Expression Patterns*, 6(8), pp. 1007–1013. Available at: https://doi.org/10.1016/j.modgep.2006.04.006.

Cajal, S.R.Y. (1893) ‘La retine des vertebres.’, *Cellule*, 9, pp. 119–255.

Cepko, C.L. *et al.* (1996) ‘Cell Fate Determination in the Vertebrate Retina’, *Proceedings of the National Academy of Sciences of the United States of America*, 93(2), pp. 589–595.

Choi, H.M.T. *et al.* (2010) ‘Programmable in situ amplification for multiplexed imaging of mRNA expression’, *Nature Biotechnology*, 28(11), pp. 1208–1212. Available at: https://doi.org/10.1038/nbt.1692.

Choi, H.M.T. *et al.* (2016) ‘Mapping a multiplexed zoo of mRNA expression’, *Development*, 143(19), pp. 3632–3637. Available at: https://doi.org/10.1242/dev.140137.

Choi, H.M.T. *et al.* (2018) ‘Third-generation in situ hybridization chain reaction: multiplexed, quantitative, sensitive, versatile, robust’, *Development*, 145(12), p. dev165753. Available at: https://doi.org/10.1242/dev.165753.

Choi, J. *et al.* (2023) ‘Spatial organization of the mouse retina at single cell resolution by MERFISH’, *Nature Communications*, 14(1), p. 4929. Available at: https://doi.org/10.1038/s41467-023-40674-3.

572 Ćorić, A. *et al.* (no date) 'A fast and versatile method for simultaneous HCR,
573 immunohistochemistry and EdU labeling (SHInE)'.

574 Easter, Jr., Stephen S. and Nicola, G.N. (1996) 'The Development of Vision in the Zebrafish
575 (Danio rerio)', *Developmental Biology*, 180(2), pp. 646–663. Available at:
576 https://doi.org/10.1006/dbio.1996.0335.

577 Fadool, J.M. (2003) 'Development of a rod photoreceptor mosaic revealed in transgenic
578 zebrafish', *Developmental Biology*, 258(2), pp. 277–290. Available at:
579 https://doi.org/10.1016/S0012-1606(03)00125-8.

580 Howard, A.G. *et al.* (2021) 'An atlas of neural crest lineages along the posterior developing
581 zebrafish at single-cell resolution', *eLife*, 10, p. e60005. Available at:
582 https://doi.org/10.7554/eLife.60005.

583 Ibarra-García-Padilla, R. *et al.* (2021) 'A protocol for whole-mount immuno-coupled hybridization
584 chain reaction (WICHCR) in zebrafish embryos and larvae', *STAR Protocols*, 2(3), p. 100709.
585 Available at: https://doi.org/10.1016/j.xpro.2021.100709.

586 Inoue, D. and Wittbrodt, J. (2011) 'One for All—A Highly Efficient and Versatile Method for
587 Fluorescent Immunostaining in Fish Embryos', *PLOS ONE*, 6(5), p. e19713. Available at:
588 https://doi.org/10.1371/journal.pone.0019713.

589 Jusuf, P.R. *et al.* (2012) 'Biasing Amacrine Subtypes in the Atoh7 Lineage through Expression of
590 Barhl2', *Journal of Neuroscience*, 32(40), pp. 13929–13944. Available at:
591 https://doi.org/10.1523/JNEUROSCI.2073-12.2012.

592 Kimura, Y., Satou, C. and Higashijima, S. (2008) 'V2a and V2b neurons are generated by the final
593 divisions of pair-producing progenitors in the zebrafish spinal cord', *Development*, 135(18), pp.
594 3001–3005. Available at: https://doi.org/10.1242/dev.024802.

595 Kroll, F. *et al.* (no date) 'A simple and effective F0 knockout method for rapid screening of
596 behaviour and other complex phenotypes', *eLife*, 10, p. e59683. Available at:
597 https://doi.org/10.7554/eLife.59683.

598 Kugler, E. *et al.* (2023) 'GliaMorph: a modular image analysis toolkit to quantify Müller glial cell
599 morphology', *Development (Cambridge, England)*, 150(3), p. dev201008. Available at:
600 https://doi.org/10.1242/dev.201008.

601 MacDonald, R.B. *et al.* (2015) 'Müller glia provide essential tensile strength to the developing
602 retina', *The Journal of Cell Biology*, 210(7), pp. 1075–1083. Available at:
603 https://doi.org/10.1083/jcb.201503115.

604 Malicki, J. *et al.* (2016) 'Chapter 8 - Analysis of the retina in the zebrafish model', in H.W. Detrich,
605 M. Westerfield, and L.I. Zon (eds) *Methods in Cell Biology*. Academic Press (The Zebrafish), pp.
606 257–334. Available at: https://doi.org/10.1016/bs.mcb.2016.04.017.

607 Masland, R.H. (2012) 'The Neuronal Organization of the Retina', *Neuron*, 76(2), pp. 266–280.
608 Available at: https://doi.org/10.1016/j.neuron.2012.10.002.

609 Ninov, N., Borius, M. and Stainier, D.Y.R. (2012) 'Different levels of Notch signaling regulate
610 quiescence, renewal and differentiation in pancreatic endocrine progenitors', *Development*,
611 139(9), pp. 1557–1567. Available at: https://doi.org/10.1242/dev.076000.

612 Patterson, B.W. *et al.* (2013) 'Visually guided gradation of prey capture movements in larval
613 zebrafish', *Journal of Experimental Biology*, 216(16), pp. 3071–3083. Available at:
614 https://doi.org/10.1242/jeb.087742.

615 Radtke, A.J. *et al.* (2020) 'IBEX: A versatile multiplex optical imaging approach for deep
616 phenotyping and spatial analysis of cells in complex tissues', *Proceedings of the National*

Academy of Sciences of the United States of America, 117(52), pp. 33455–33465. Available at: https://doi.org/10.1073/pnas.2018488117.

Robinson, J., Schmitt, E.A. and Dowling, J.E. (1995) 'Temporal and spatial patterns of opsin gene expression in zebrafish (Danio rerio)', *Visual Neuroscience*, 12(5), pp. 895–906. Available at: https://doi.org/10.1017/S0952523800009457.

Santos, D., Monteiro, S.M. and Luzio, A. (2018) 'General Whole-Mount Immunohistochemistry of Zebrafish (Danio rerio) Embryos and Larvae Protocol', *Methods in Molecular Biology (Clifton, N.J.)*, 1797, pp. 365–371. Available at: https://doi.org/10.1007/978-1-4939-7883-0_19.

Vitorino, M. *et al.* (2009) 'Vsx2 in the zebrafish retina: restricted lineages through derepression', *Neural Development*, 4(1), p. 14. Available at: https://doi.org/10.1186/1749-8104-4-14.

Wang, J. *et al.* (2017) 'Anatomy and spatial organization of Müller glia in mouse retina', *The Journal of Comparative Neurology*, 525(8), pp. 1759–1777. Available at: https://doi.org/10.1002/cne.24153.

Westerfield, M. (1993) *The Zebrafish Book: A Guide for the Laboratory Use of Zebrafish (Brachydanio Rerio)*. M. Westerfield.

White, D.T. *et al.* (2017) 'Immunomodulation-accelerated neuronal regeneration following selective rod photoreceptor cell ablation in the zebrafish retina', *Proceedings of the National Academy of Sciences*, 114(18), pp. E3719–E3728. Available at: https://doi.org/10.1073/pnas.1617721114.

Williams, P.R. *et al.* (2010) 'In vivo development of outer retinal synapses in the absence of glial contact', *The Journal of Neuroscience: The Official Journal of the Society for Neuroscience*, 30(36), pp. 11951–11961. Available at: https://doi.org/10.1523/JNEUROSCI.3391-10.2010.

639 Yazulla, S. and Studholme, K.M. (2001) ‘Neurochemical anatomy of the zebrafish retina as
640 determined by immunocytochemistry’, *Journal of Neurocytology*, 30(7), pp. 551–592. Available
641 at: https://doi.org/10.1023/a:1016512617484.

642 Zolessi, F.R. *et al.* (2006) ‘Polarization and orientation of retinal ganglion cells in vivo’, *Neural*
643 *Development*, 1(1), p. 2. Available at: https://doi.org/10.1186/1749-8104-1-2.

644

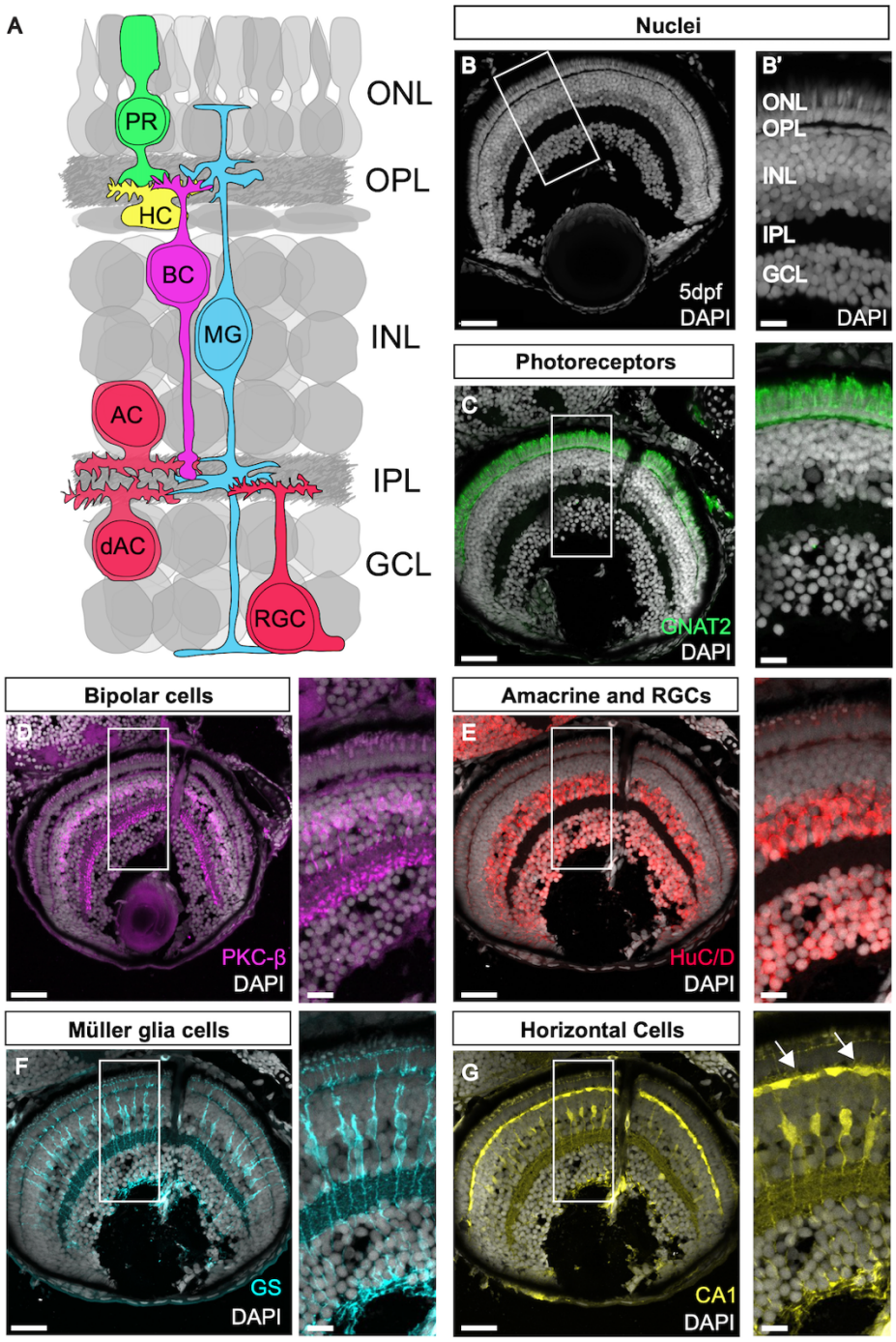

Figure 1. The retina is made up of highly organised layers composed of neurons and glia. (A) Schematic of the retina showing the layers and major cell populations with each cell type colour coded. (B) DAPI staining showing the nuclear layers of the retina. (B') Zoom of B. (C-G) Antibody staining for the main cell types in the zebrafish retina. Arrows in G show horizontal cells.

650 OLM: outer limiting membrane, ONL: outer nuclear layer, OPL: outer plexiform layer, INL: inner
651 nuclear layer, IPL: inner plexiform layer, GCL: ganglion cell layer. Scale bars - 25μm for whole
652 retina, 10μm for zoom images.
653

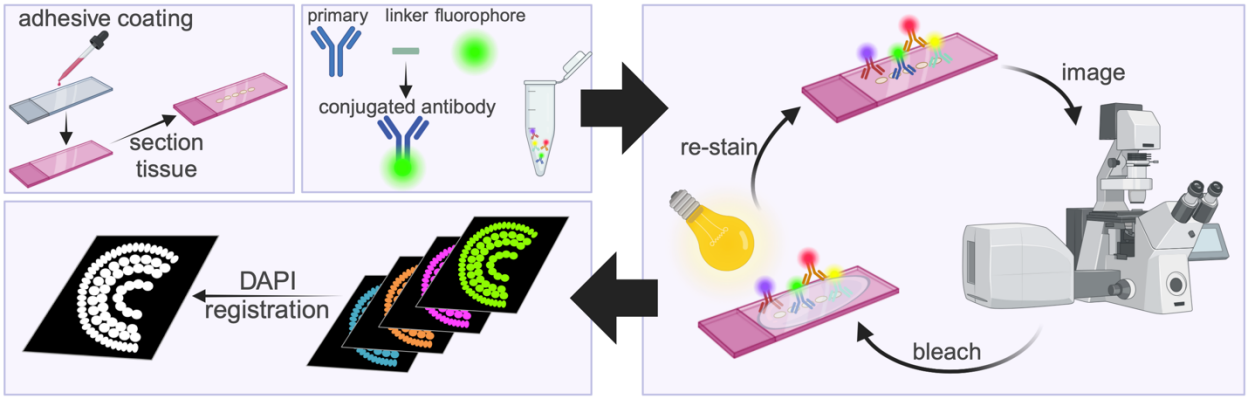

Figure 2. Schematic of the IBEX method. Slides are coated with chrome alum gelatin to prevent tissue lost, then tissue sectioned onto slides. Antibodies are micro-conjugated by mixing the primary antibody with a linker and fluorophore. The antibodies are applied to the slide, incubated, imaged, then bleached using bright light and lithium borohydride before being re-stained. After the imaging rounds are completed, nuclear stains (DAPI) are used to register the image, allowing for all stains to be visualised together. Made with Biorender.

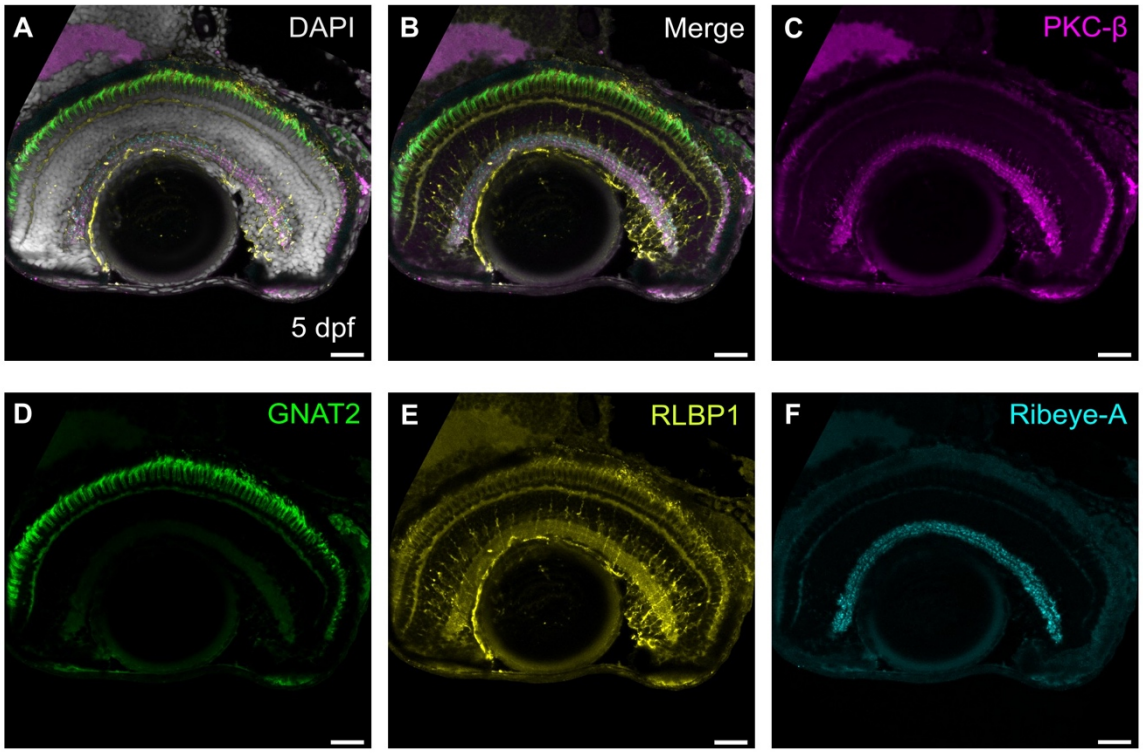

667

668 **Figure 3. Direct conjugation to fluorophores facilitates multiple single species antibody**
669 **labels on the same tissue.** (A) Merged epifluorescence images of a single sagittal retinal section
670 immunolabelled with four antibodies raised in rabbit: PKC-β (magenta), GNAT2 (green), RLBP1
671 (yellow), Ribeye-A (cyan), and nuclear stain DAPI (grey). (B) Merged image without DAPI. (C)
672 Retinal section immunolabelled with PKC-β, marking bipolar cells. (D) Retinal section
673 immunolabelled with GNAT2 marking cones. (E) Retinal section immunolabelled with RLBP1,
674 marking Müller glia cells. (F) Retinal section immunolabelled with Ribeye-A marking ribbon
675 synapses. Scale bars - 25μm

676

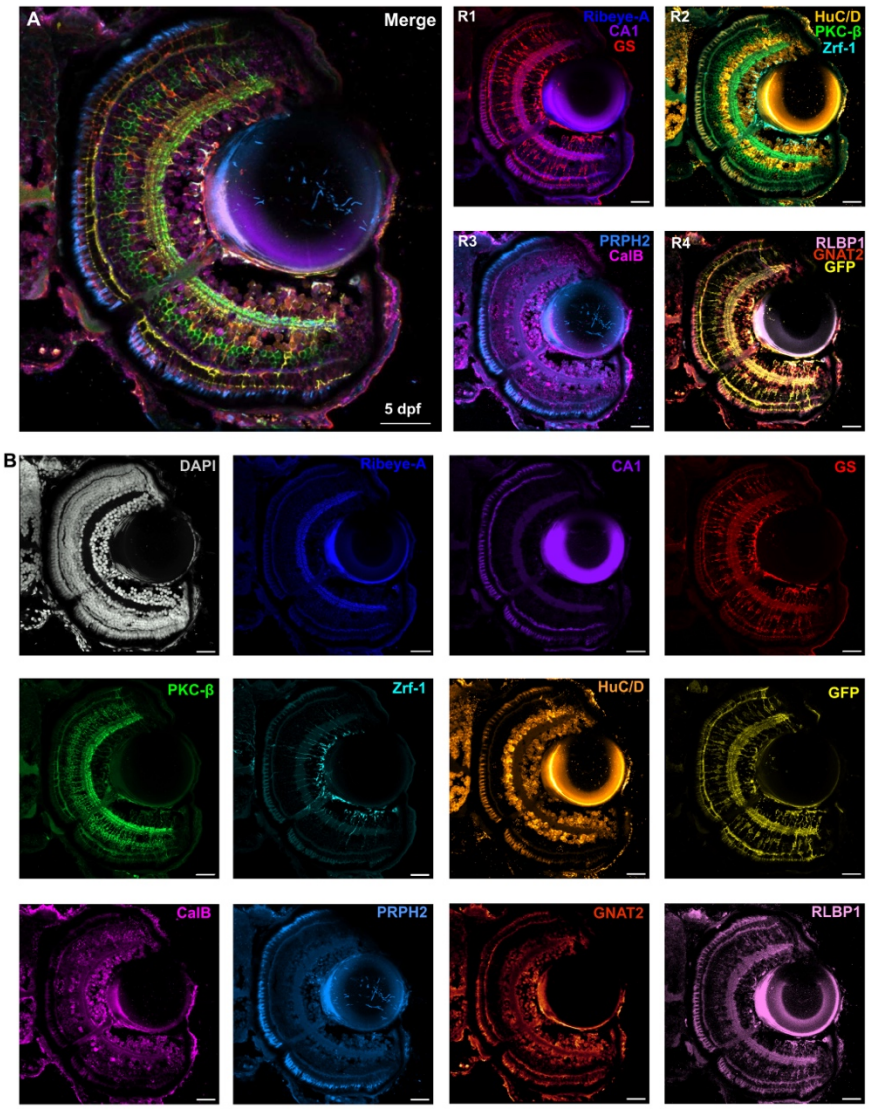

Figure 4. IBEX enables simultaneous labelling of all retinal cell types. (A) Confocal images of 5 dpf Tg(*tp1:eGFP:CAAX*) zebrafish retina showing different rounds of immunolabelling (R1-4) using IBEX and the merge composite image of each of these rounds. R1 was carried out using Alexa Fluor secondary antibodies, while other rounds used microconjugated antibodies. (B) Confocal images showing each antibody used in (A) to immunolabel a single sagittal retinal section with DAPI and 11 different markers: Ribeye-A (dark blue), carbonic anhydrase (CA1, purple), glutamine synthetase (GS, red), PKC-β (green), Zrf-1 (cyan), HuC/D (orange), GFP

685 transgene (yellow), calbindin (CalB, magenta), peripherin-2 (PRPH2, light blue), GNAT2 (orange),
686 and RLBP1 (pink). Scale bars - 25μm.
687
688
689
690
691
692
693

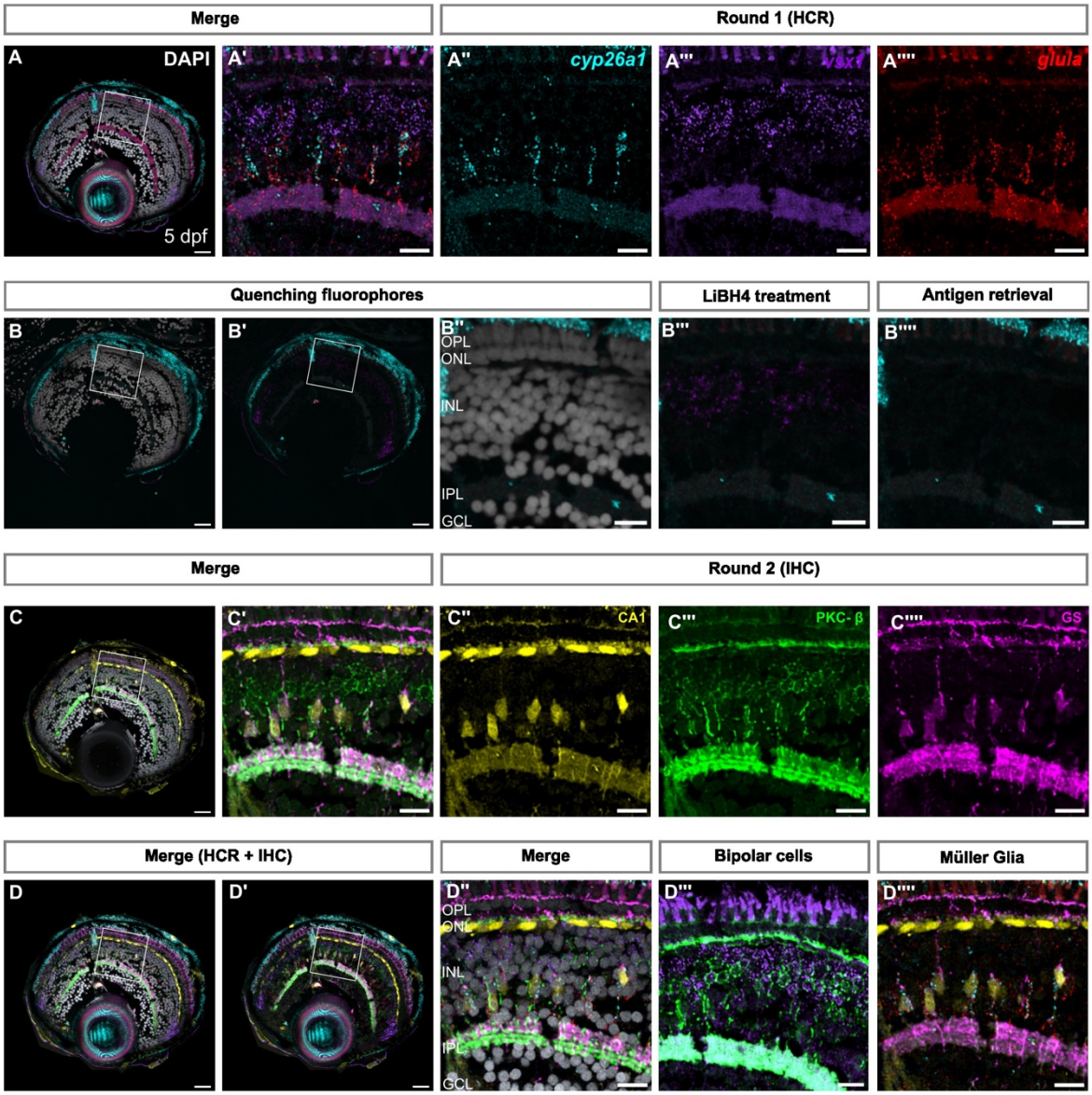

Figure 5. IBEX is compatible with fluorescent *in situ* hybridisation chain reaction. (A) Confocal images of retinal sections showing mRNA expression of *cyp26a1*, *glula*, and *vsx1*, using *in situ* hydridisation chain reaction (HCR). (A′-A′′′′) Zoom on the region of interest indicated in (A). (B-B′′′) Confocal images showing reduced signal of Alexa Fluor-488 and Alexa Fluor-647, but not Alexa Fluor-555 after LiBH4 treatment. (B′′′′) Heating in sodium citrate at 60ºC causes inactivation of Alexa Fluor 555 as well as Alexa Fluor 488 and Alexa Fluor 647. (C) Confocal images of retinal sections immunolabelled with CA1 (yellow), PKC-β (green), and GS (magenta). (C′ -C′′′) Zoom on

702 region of interest indicated in (C). (D) SimpleITK registered image, showing overlay of both rounds
703 of imaging, and overlay of *in situ* probes and antibodies detecting Müller glia and bipolar cells,
704 respectively. (D″-D‴) Zoom of region of interest shown in (D,D′). GCL: ganglion cell layer, IPL:
705 inner nuclear layer, ONL: outer nuclear layer, OPL: outer plexiform layer. Scale bars - 25μm for
706 whole retina, 10μm for zoom images.

707

708

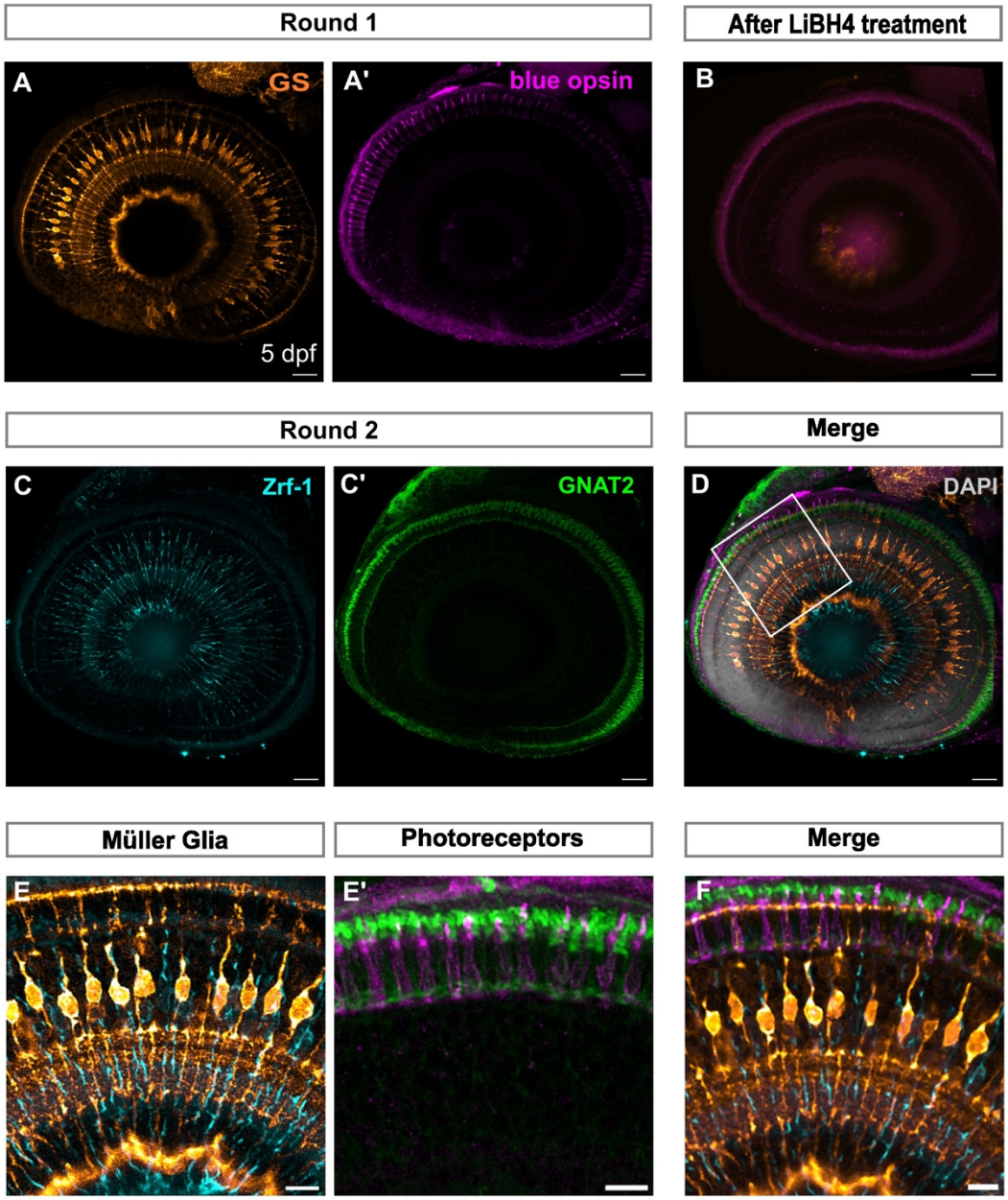

709

710 **Figure 6. Wholemount IBEX facilitates whole tissue labelling in zebrafish** (A,A′) Confocal
711 images of wholemount zebrafish larvae at 5 dpf immunolabelled with GS (orange) and blue opsin
712 (magenta). (B) Tissue after bleaching with LiBH4 showing reduced signal of fluorophores CoraLite
713 488 and CoraLite 647. (C,C′) Confocal images of the second round of immunolabelling to detect
714 Zrf-1 (cyan) and GNAT2 (green). (D) Merge of both rounds of immunolabelling using SimpleTK
715 registration pipeline counterstained with DAPI (grey). (E) Overlap of MG markers GS and Zrf-1

716 across round 1 and 2. (E′) Overlap of photoreceptor markers blue opsin and GNAT2 across round
717 1 and 2. (F) Zoom in of (D), showing overlay of MG and photoreceptor labelling. dpf: days post
718 fertilisation, MG: Müller glia. Scale bars - 25μm for whole retina, 10μm for zoom images.
719
720
721
722
723
724

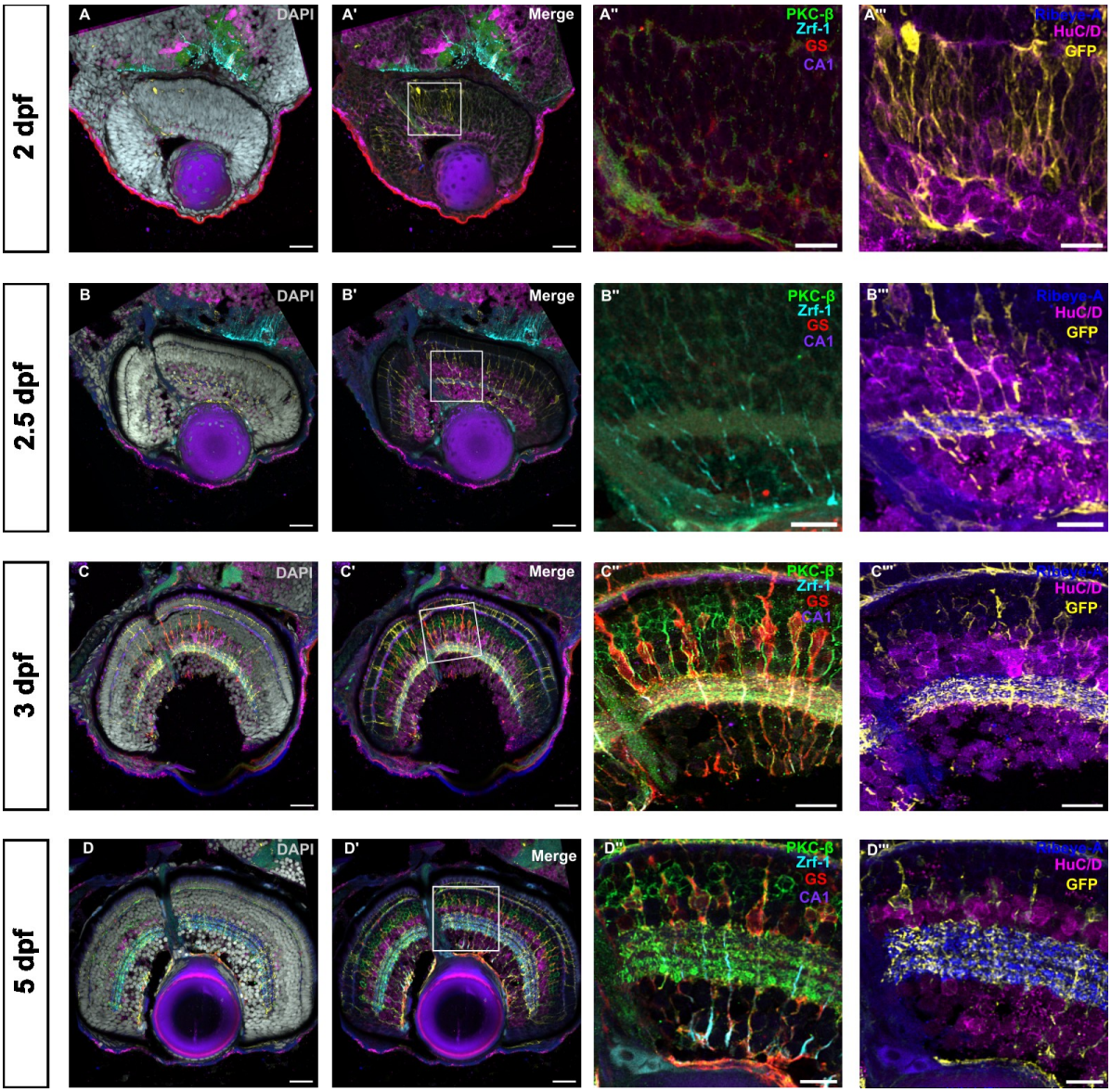

Figure 7. Visualisation of glial and neuronal development in the zebrafish retina. Confocal images of the developing zebrafish retina from 2 dpf to 5 dpf immunolabelled with DAPI and 7 different markers using IBEX over 3 rounds of immunolabelling with IBEX. A, B,C,D show merge of all 7 markers with nuclear stain DAPI, while A′,B′,C′,D′ show the same overlay of markers without DAPI. A″,B″,C″,D″ show the first 2 rounds of immunolabelling of bipolar cells (PKC-β, green), glial intermediate filaments (Zrf-1, cyan), horizontal cells (CA1, purple) and Müller glia (GS, red) at different timepoints. A‴,B‴,C‴,D‴ show the last round of immunolabelling of ribbon

734 synapses (Ribeye-A, blue), amacrine and ganglion cells (HuC/D, magenta) and Müller glia (eGFP
735 transgene, yellow) at different, crucial timepoints of retinal development (2, 2.5, 3, and 5 dpf)
736 showing retinal progenitors in (A-A‴). (B-B‴) shows nascent IPL and Müller glia formation. In (C-
737 C‴ and D-D‴), IPL sublamination and Müller glia elaboration is evident. dpf: days post fertilisation,
738 IPL: inner plexiform layer. Scale bars - 25μm for whole retina, 10μm for zoom images.
739

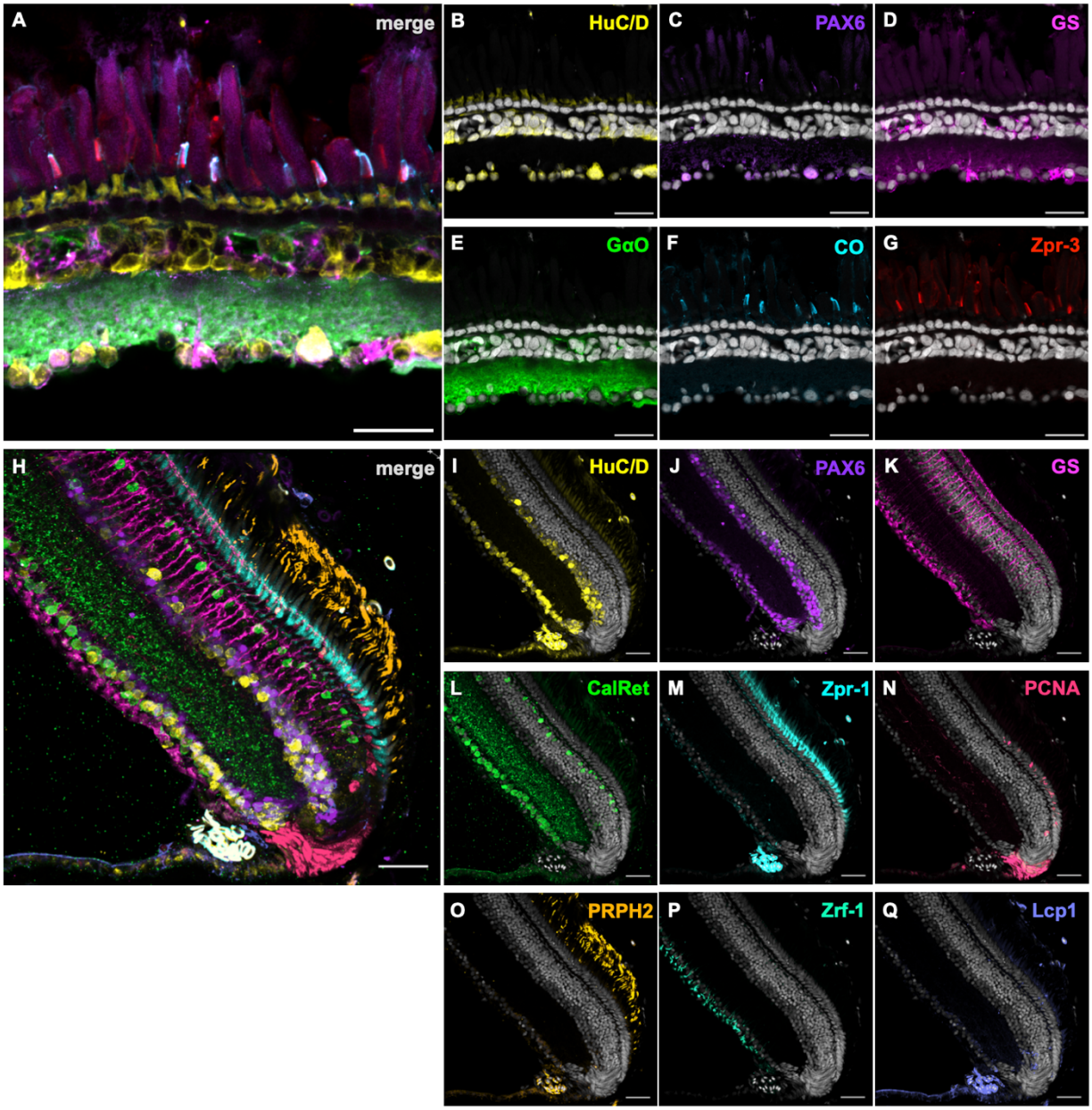

Figure 8. IBEX on African clawed frog and turquoise killifish retina. (A) 5-month-old *Xenopus laevis* tadpole sagittal retinal sections labelled with HuC/D (B, yellow), PAX6 (C, purple), GS (D, magenta), GαO (E, green), cone opsin (F, cyan), and zpr-3 (G, red). HuC/D labelled cells within the GCL and amacrine cell sublayer, as well as photoreceptor inner segments. PAX6 labelled primarily cells within the GCL, likely RGCs and/or displaced amacrine cells. Müller glia were labelled with GS. GαO labelled bipolar cell bodies and processes within the INL and IPL, respectively. L/M cone outer segments were co-labelled with CO and zpr-3. (H) 8-week old adult

748 killifish retinal sections labelled with HuC/D (I, yellow), PAX6 (J, purple), GS (K, magenta),
749 Calretinin (L, green), Zpr-1 (M, cyan), PCNA (N, red), PRPH2 (O, orange), Zrf-1 (P, light green),
750 and Lcp1 (Q, lavender/light purple). Huc/D and PAX6 labelled cells within the GCL and amacrine
751 cell sublayer, as seen in zebrafish and frogs. GS and zrf-1 labelled Müller glia. Calretinin labelled
752 cells within the GCL and amacrine cell sublayer. Zpr-1 labelled entire double cone cells, and
753 PRPH2 labelled photoreceptor outer segments. PCNA expression was observed in the CMZ and
754 in the photoreceptor cell layer. Lcp1 was observed in the INL, close to the CMZ, and within the
755 photoreceptor cell layer. GCL: ganglion cell layer. INL: inner nuclear layer. IPL: inner plexiform
756 layer. RGC: retinal ganglion cell. Scale bars - 25μm for *Xenopus*; 30μm for killifish.
757
758
759
760
761
762
763
764
765
766
767
768
769
770
771
772
773

774 SUPPLEMENTAL FIGURES

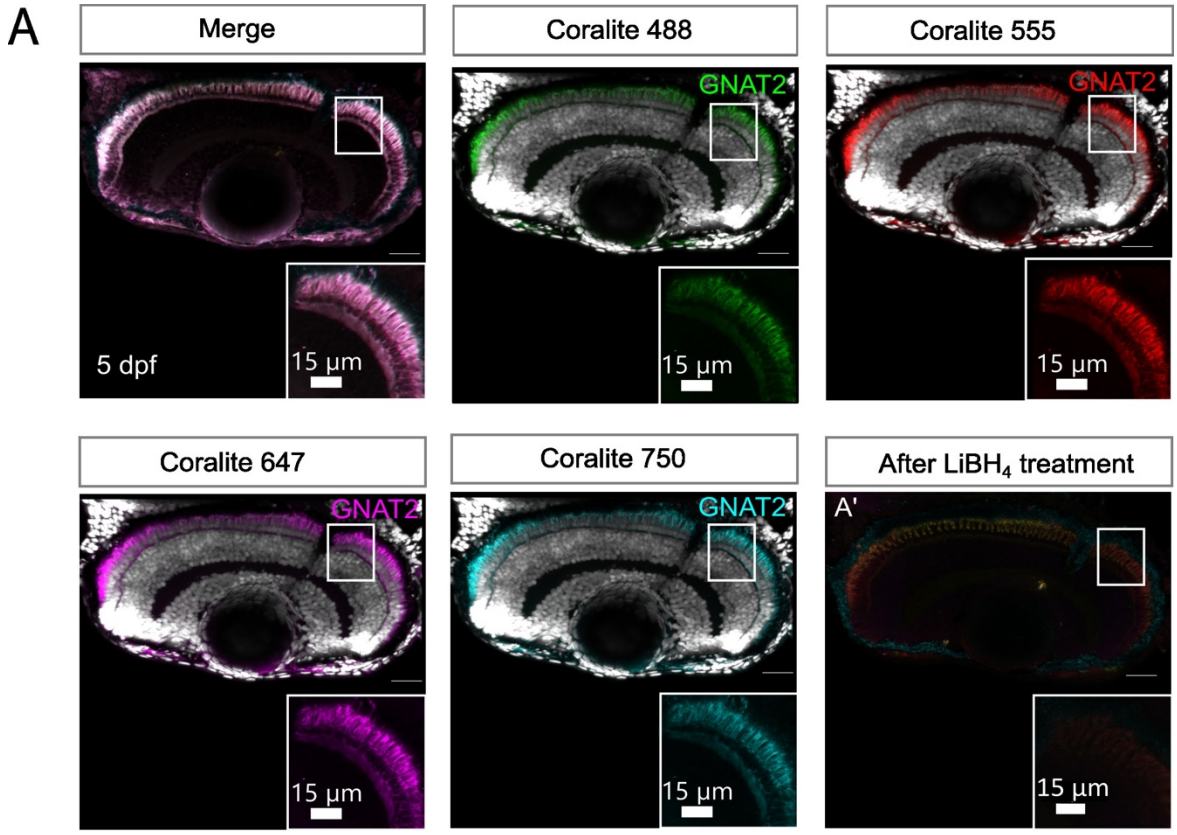

775

776 **Supplemental Figure 1.** (A) Epifluorescence images of cone photoreceptor cells immunolabelled
777 with the GNAT2 antibody on the same single retinal section. Rabbit α-GNAT2 is conjugated to
778 Coralite 488, Coralite 550, Coralite 647 and Coralite 750. (A′) Decreased signal after bleaching
779 the sample with LiBH4 under bright light. Scale bars - 40µm for whole retina, 15µm for zoom
780 images.

781

782

783

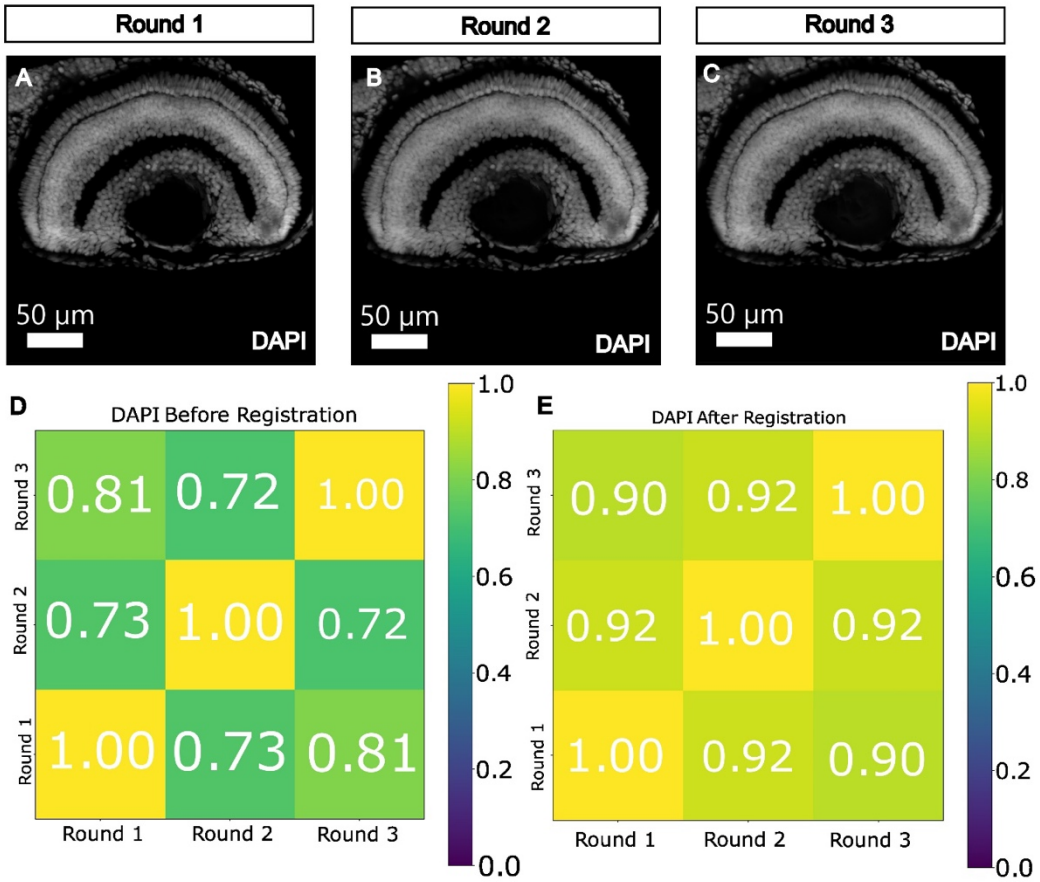

Supplemental Figure 2. Three round IBEX run on 5 dpf zebrafish retina cryosections with Z-stacks using a 63x objective and 2x optical zoom on the Leica SP8 confocal microscope (three separate technical repeats were performed). (A-C) Maximum projections of DAPI staining during the imaging of rounds 1-3, respectively. (D) Correlation matrix for DAPI staining across the rounds before Simple ITK registration of Z-stacks. (E) Correlation in DAPI staining across the rounds after affine registration of Z-stacks. Scale bars - 50µm.

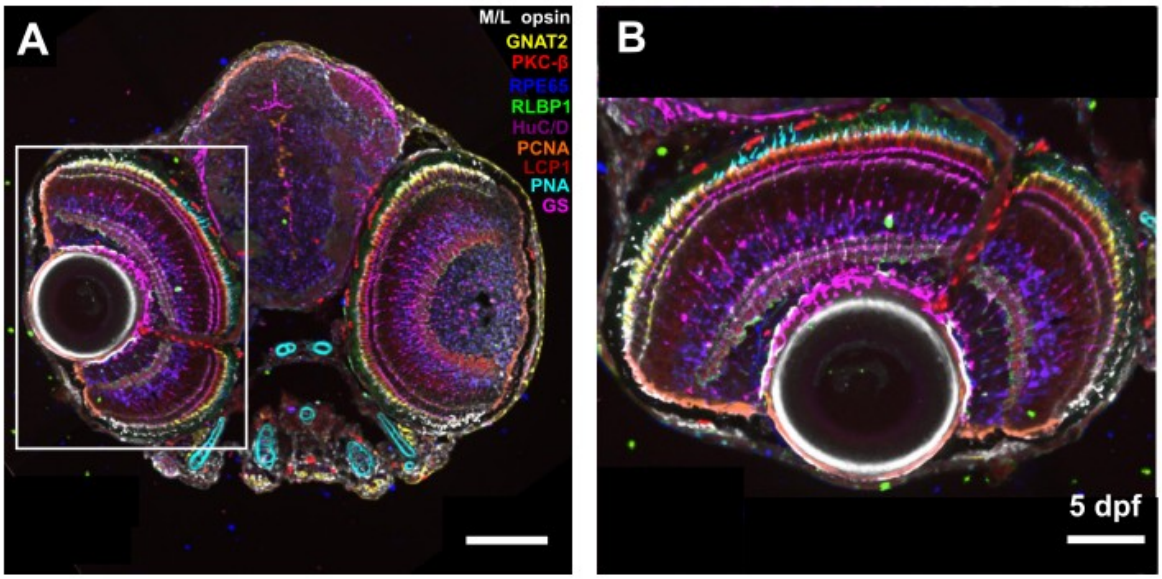

Supplemental Figure 3. Three round IBEX run using the Leica THUNDER imager with a 40x air objective following instant computational clearing.(A) Epifluorescence images of 5dpf zebrafish retinal section immunolabelled with a panel of 9 antibodies and a lectin stain: RPE65 (dark blue), GS (magenta), PKC-β (red), HuC/D (purple), PCNA (orange), GNAT2 (yellow), RLBP1 (green), Lcp-1 (maroon), M/L opsin (white) and PNA stain (cyan). (B) Zoom in of region of interest indicated in A, with merge of the 10 antibodies used. Scale bar - 80μm (A) and 40μm (B).

807

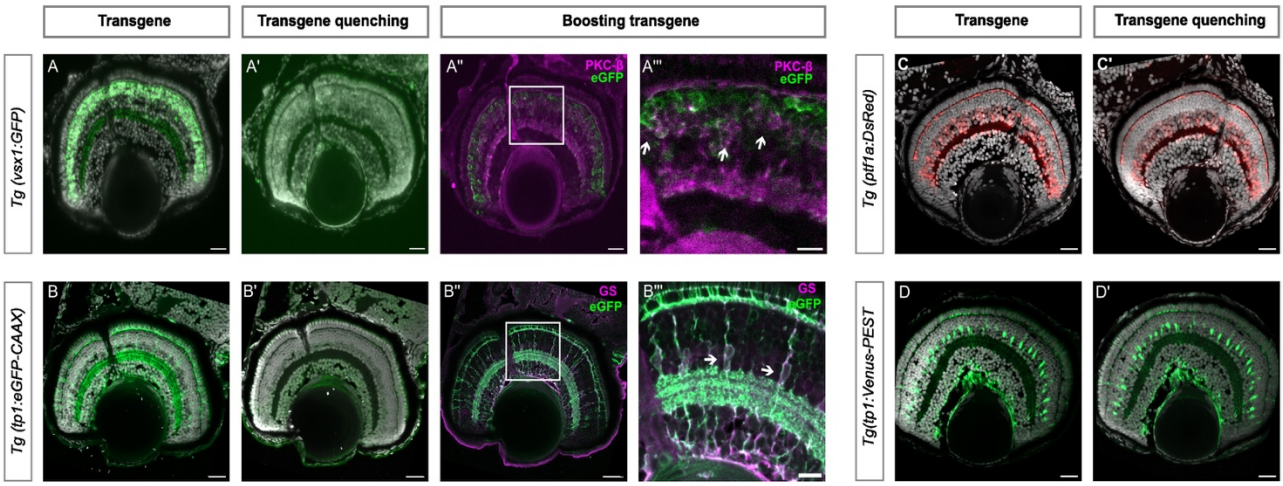

808

809 **Supplemental Figure 4. IBEX is compatible with transgenic fluorescent reporter lines.** (A)
810 Images of 5 dpf cytosolic GFP (Tg(*vsx1:GFP*) transgenic labelling bipolar cells) positive retinal
811 sections without any treatment. (A′) Images of the same section after sodium citrate treatment,
812 showing reduced signal. (A″) Section imaged after boosting transgene with anti-GFP antibody
813 and co-labelling with PKCβ to confirm specificity of boosted transgene. (A‴) Zoom in of region of
814 interest in (A″). (B) Confocal images of 5 dpf membrane bound GFP (Tg(*tp1:eGFP-CAAX*)
815 transgenic labelling MG membranes) positive retinal sections without any treatment. (B′) Images
816 of the same section after sodium citrate treatment, showing reduced signal. (B″) Section imaged
817 after boosting transgene with anti-GFP antibody and co-labelling with GS to confirm specificity of
818 transgene (zoom: arrows). (B‴) Zoom of region of interest indicated in (B″). (C, D) Confocal
819 images of RFP (Tg(*ptf1a:Dsred*) transgenic) and YFP (Tg(*tp1:Venus-PEST*) transgenic retinal
820 sections without treatment. (C′,D′) RFP and YFP transgenes do not show any change in signal
821 after sodium citrate treatment. dpf: days post fertilisation, MG: Müller glia. Scale bar -25μm.

822

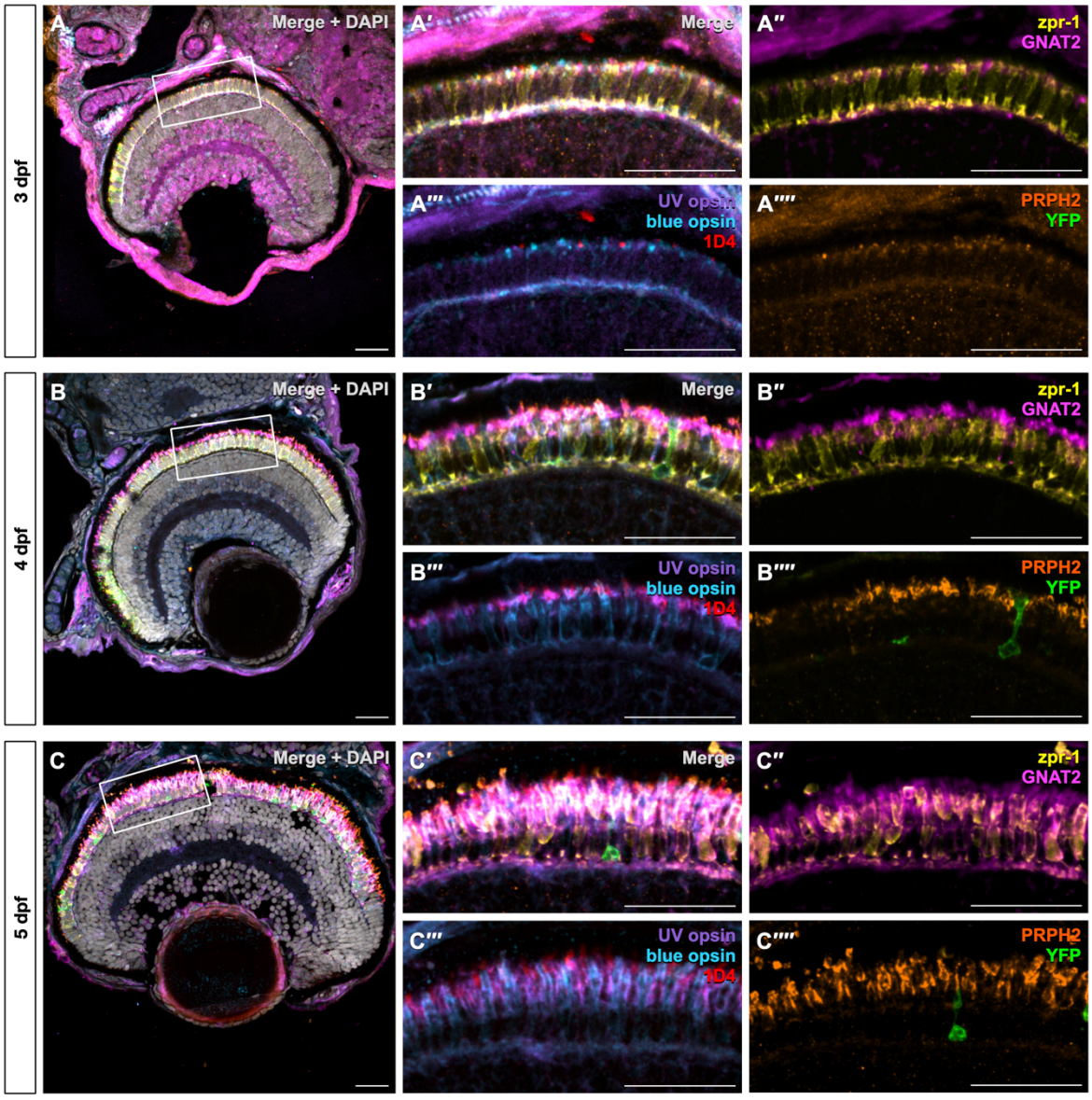

Supplemental Figure 5. Visualisation of all photoreceptor subtypes during zebrafish development using IBEX. Sagittal sections of Tg(*rho:YFP*) embryos labelled with zpr-1 (yellow), GNAT2 (pink), UV opsin (purple), blue opsin (blue), 1D4 (red), and PRPH2 (orange) at 3 (A), 4 (B), and 5 (C) dpf. YFP is shown in green. (A′, B′, C′) Show zooms of photoreceptors will all labels merged, without DAPI; (A″, B″, C″) shows zpr-1 and GNAT2 labelling; (A‴, B‴, C‴) shows UV, blue, and red opsin (1D4) labelling; and (A⁗, B⁗, C⁗) shows PRPH2 labelling and YFP. (A) 3 dpf retinas have small, newly developing outer segments visible by UV opsin, blue opsin, red opsin

(1D4), and PRPH2 labelling. Entire cone cell bodies are visible by GNAT2 labelling, while red and green cone cell bodies are visible by arrestin 3a (zpr-1) labelling. Newly formed rods are visible at the periphery of the retina by YFP labelling. (B) 4 dpf embryos have longer outer segments with increased PRPH2 staining indicative of disc structure. (C) 5 dpf embryos have long outer segments that are visibly starting to taper into more of a “cone-like” morphology. Scale bars - 25μm.

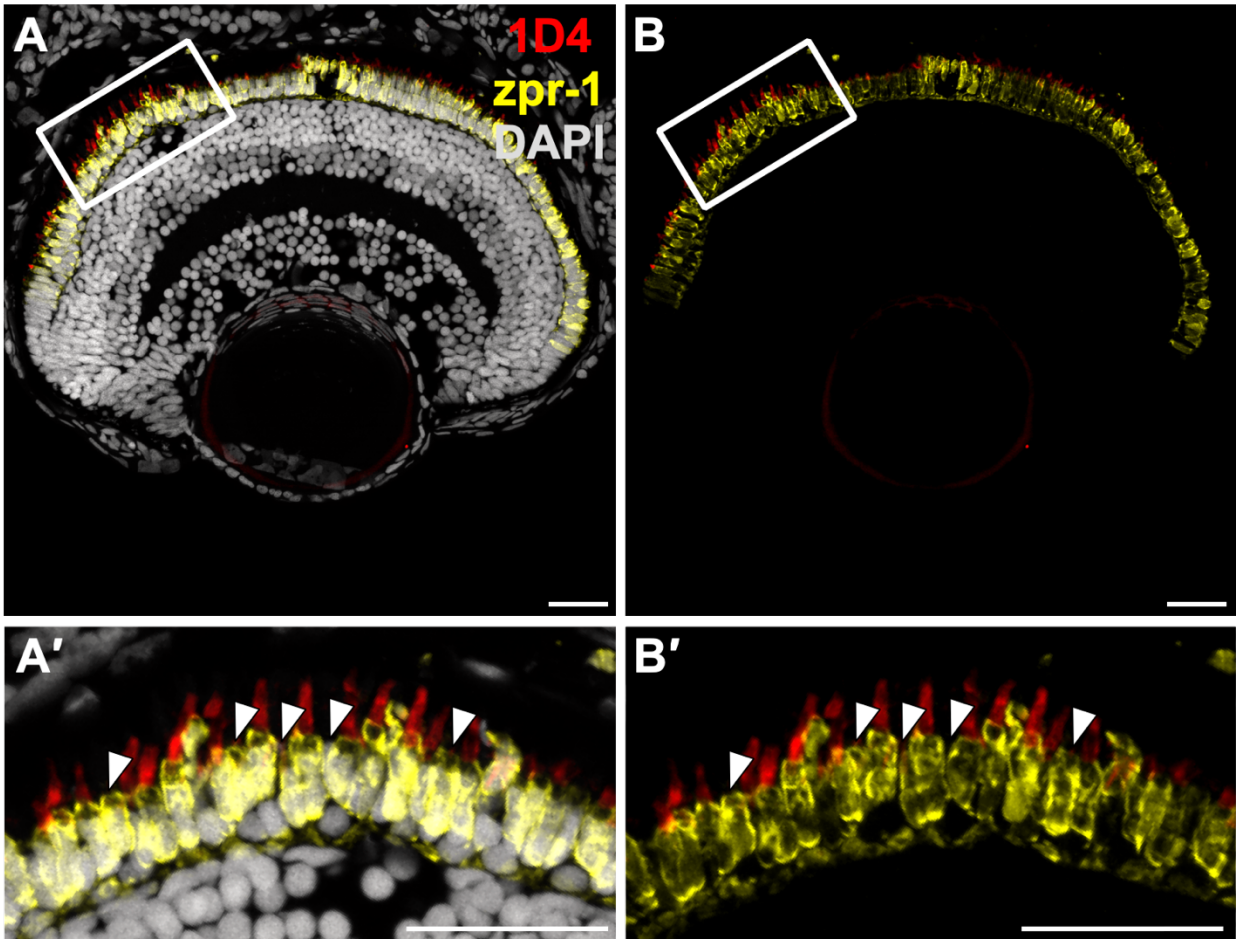

Supplemental Figure 6. Discrimination of green cones in 5 dpf zebrafish retina. Red cones are positive for both zpr-1 and 1D4 (red opsin), whereas green cones are positive for only zpr-1 (arrowheads). Scale bars - 25μm.